

Adaptive Bayesian Sum of Trees Model for Covariate Dependent Spectral Analysis

Yakun Wang¹, Zeda Li², and Scott A. Bruce^{1,*}

¹Department of Statistics, George Mason University, Fairfax, Virginia, U.S.A.

²Paul H. Chook Department of Information System and Statistics,
Baruch College, The City University of New York, New York, New York, U.S.A.

**email*: sbruce7@gmu.edu

SUMMARY: This article introduces a flexible and adaptive nonparametric method for estimating the association between multiple covariates and power spectra of multiple time series. The proposed approach uses a Bayesian sum of trees model to capture complex dependencies and interactions between covariates and the power spectrum, which are often observed in studies of biomedical time series. Local power spectra corresponding to terminal nodes within trees are estimated nonparametrically using Bayesian penalized linear splines. The trees are considered to be random and fit using a Bayesian backfitting Markov chain Monte Carlo (MCMC) algorithm that sequentially considers tree modifications via reversible-jump MCMC techniques. For high-dimensional covariates, a sparsity-inducing Dirichlet hyperprior on tree splitting proportions is considered, which provides sparse estimation of covariate effects and efficient variable selection. By averaging over the posterior distribution of trees, the proposed method can recover both smooth and abrupt changes in the power spectrum across multiple covariates. Empirical performance is evaluated via simulations to demonstrate the proposed method's ability to accurately recover complex relationships and interactions. The proposed methodology is used to study gait maturation in young children by evaluating age-related changes in power spectra of stride interval time series in the presence of other covariates.

KEY WORDS: Bayesian backfitting; Gait variability; Multiple time series; Reversible jump Markov chain Monte Carlo; Spectrum analysis; Whittle likelihood.

1. Introduction

The frequency-domain properties of time series have often been found to contain valuable information. For example, frequency-domain analysis of biomedical time series, such as gait variability, heart rate variability (HRV), and electroencephalography (EEG), provides interpretable information about underlying physiological processes (Hausdorff et al., 1999; Hall et al., 2004; Klimesch, 1999). In many studies, biomedical time series are collected from multiple participants in conjunction with multiple covariates to explore connections between prominent oscillatory patterns in the time series and various clinical and behavioral outcomes. These relationships are often complex and highly interactive. As a result, a flexible, adaptive method that can estimate the association between power spectra and multiple covariates is needed to better understand the complex relationships between physiological processes and important measures of health and functioning.

A prime example and motivating application for this article comes from a study of maturation in gait dynamics in young children (Hausdorff et al., 1999). Immature gait in very young children results in unsteady walking patterns and frequent falls (Brenière and Bril, 1988; Shumway-Cook and Williams, 1995). While gait is relatively mature by age 3, neuromuscular control continues to develop well beyond this age (Shumway-Cook and Williams, 1995; Preis et al., 2008). Accordingly, it is of interest to assess if gait dynamics continue to become more steady and regular beyond age 3, in conjunction with improving neuromuscular control. To assess gait variability and posture control in younger children, stride interval time series consisting of stride times during normal walking were observed in fifty children between the ages of 3 and 14 (Hausdorff et al., 1999). For illustration, Figure 1 displays demeaned stride interval time series for three participants age 4, 7, and 11 years old. In addition to age, other covariates were also collected that may influence gait, such as gait speed and gender. In quantifying the association between age and the power spectra of stride interval time series,

we seek to better understand the maturation of gait dynamics and variability associated with developing neuromuscular control with age in the presence of other related covariates.

[Figure 1 about here.]

In the time series literature, spectral analysis of multiple time series has received much attention in recent years. To quantify the association between a *single* covariate and power spectra, Fiecas and Ombao (2017) and Krafty et al. (2017) propose methods that can capture a smooth covariate effect on the power spectrum. Bruce et al. (2018) proposes an adaptive Bayesian method that can capture both smooth and abrupt changes in power spectra across a covariate. Li et al. (2021) adapts the method of Bruce et al. (2018) for covariate-dependent spectral analysis of replicated multivariate time series. However, these methods are not readily extendable to incorporate *multiple* covariates, which hinders their applicability to many important studies. Existing methods that can account for multiple covariates are either parametric (Diggle and Al Wasel, 1997) or semi-parametric (Iannaccone and Coles, 2001; Qin et al., 2009; Stoffer et al., 2010; Krafty et al., 2011; Chau and von Sachs, 2016). These approaches characterize covariate effects via design matrices within a linear modeling framework, and thus can not immediately accommodate complex dependencies and interactions among covariates and power spectra. One exception is the approach proposed by Bertolacci et al. (2019), which introduces a mixture modeling approach with covariate-dependent mixture weights to account for complex covariate effects. However, a thin-plate Gaussian process prior is imposed on mixture weights, which is both smooth and stationary, and may not be appropriate for modeling abrupt spectral dynamics. Moreover, this method does not provide a means for variable selection when a large number of covariates are observed. The goal of this article is to introduce a flexible method that can capture both smooth and abrupt changes in power spectra across multiple covariates, without loss of interpretation, and simultaneously provide a tool for variable selection.

To capture complex smooth, abrupt, and interaction effects of covariates on power spectra in a parsimonious manner, we propose a tree-based covariate partitioning framework. Tree-based models are not new and have become extremely popular in recent years (Breiman, 2001; Chipman et al., 2010). For example, Chipman et al. (2010) propose a Bayesian additive regression tree (BART) model which can flexibly model complex covariate effects and interactions and demonstrates outstanding predictive performance (Chipman et al., 2013). Accordingly, BART has been widely applied in many different scientific domains for various types of outcomes (Waldmann, 2016; Blattenberger and Fowles, 2017; van der Merwe, 2018) including smooth functional response variables (Starling et al., 2020).

In this article, a sum of trees model for the covariate-dependent power spectrum is introduced to simultaneously partition multiple covariates parsimoniously. A penalized linear spline model is used for local spectrum estimation within terminal nodes of the trees. The framework is formulated in a fully Bayesian setting where the trees are random and fit using an iterative Bayesian backfitting Markov chain Monte Carlo (MCMC) procedure and reversible-jump techniques (Green, 1995) to evaluate various tree modifications.

The proposed methodology expands the scope of covariate dependent power spectra that can be accurately recovered in three meaningful ways. First, the flexible sum of trees model can recover complex nonlinear relationships and interaction effects without assuming a particular form of the relationship a priori. Second, by averaging over the posterior distribution of trees, the proposed method can recover both smooth and abrupt covariate effects on the power spectrum. Third, the proposed method can automatically accommodate mixed-type covariates (nominal, ordinal, discrete, continuous) through the underlying tree structures, as well as high-dimensional covariates by placing a sparsity-inducing Dirichlet hyperprior on the splitting proportions of the regression tree prior (Lineró, 2018) for sparse estimation of covariate effects and variable selection.

The rest of the paper is organized as follows. Section 2 provides a definition for the covariate-dependent power spectrum. The tree-based modeling framework for the power spectrum is introduced in Section 3, and Section 4 proposes the adaptive Bayesian sum of trees model and MCMC sampling scheme. Simulation results for various covariate effects (e.g. linear, nonlinear, smooth, abrupt, high-dimensional) and interaction effects are provided in Section 5. Section 6 presents the application to the study of gait maturation in young children. Conclusions and future directions of this work are covered in Section 7.

2. Covariate-Dependent Power Spectrum

We consider modeling a collection of stationary time series $X_{\ell t}$ of length $t = 1, \dots, T$ and P -dimensional covariate vectors $\boldsymbol{\omega}_\ell = (\omega_{1\ell}, \dots, \omega_{P\ell})'$ for $p = 1, \dots, P$ mixed-type covariates and $\ell = 1, \dots, L$ independent subjects. To evaluate the effect of multiple covariates on the power spectrum, an extension of the Cramér representation (Cramér, 1942) is considered, which allows the power spectrum to vary across frequencies and covariates

$$X_{\ell t} = \int_{-1/2}^{1/2} A(\boldsymbol{\omega}_\ell, \nu) \exp(2\pi i t \nu) dZ_\ell(\nu),$$

where $A(\boldsymbol{\omega}_\ell, \nu)$ is a Hermitian and periodic complex-valued function of frequency $\nu \in \mathbb{R}$ and covariates $\boldsymbol{\omega}_\ell$ such that $A(\boldsymbol{\omega}_\ell, \nu) = \overline{A(\boldsymbol{\omega}_\ell, -\nu)}$, $A(\boldsymbol{\omega}_\ell, \nu) = A(\boldsymbol{\omega}_\ell, \nu + 1)$, and $A(\boldsymbol{\omega}_\ell, \nu)$ is square integrable over frequencies $[-1/2, 1/2]$. Z_ℓ are zero-mean mutually independent and identically distributed orthogonal processes with unit variance. Regularity conditions on the distribution of Z_ℓ must also be assumed to ensure subsequently introduced estimators are well-behaved; we assume cumulants of dZ_ℓ exist and are bounded for all orders (Brillinger, 2002).

The covariate-dependent power spectrum is then defined as $f(\boldsymbol{\omega}, \nu) = |A(\boldsymbol{\omega}, \nu)|^2$ and can be interpreted as the contribution to the variance at frequency ν given covariate values $\boldsymbol{\omega}$. We assume that A , and subsequently the spectrum f , are continuous functions of frequency

ν , but can have a finite number of discontinuities as functions of covariates ω . This flexibility allows for modeling abrupt changes over the covariate space and differs from models assuming entirely smooth changes across covariates (Fiecas and Ombao, 2017; Krafty et al., 2017).

3. Tree-Based Modeling of the Power Spectrum

3.1 Tree-Based Piecewise Stationary Approximation

The covariate-dependent power spectrum introduced in Section 2 can be approximated by piecewise stationary processes via partitioning the covariate space into approximately stationary blocks. Piecewise stationary approximations of the power spectrum have been well-studied within the context of nonstationary time series analysis (Adak, 1998; Rosen et al., 2012), where time series are divided into approximately stationary intervals for time-dependent spectral analysis. Bruce et al. (2018) introduced a time- and covariate-based piecewise stationary approximation for time- and covariate-dependent spectral analysis using a two-dimensional grid.

However, directly extending a two-dimensional grid to higher dimensions in order to accommodate multiple covariates can easily lead to over-parameterization and undue computational complexity. Tree-based approaches represent a more flexible and parsimonious alternative for partitioning multiple covariates. A grid-based partition tends to produce a finer partition than is necessary, since partition points for each covariate do not depend on the other covariate. This results in less efficient information sharing across series with similar covariates and less accurate estimation. Conversely, if the true partition does have a grid structure, a tree-based model can still well-approximate the partition and is thus preferable.

For tree-based piecewise stationary approximation, each terminal node is defined through a collection of splitting rules corresponding to the tree structure and represents an approxi-

mately stationary region of the covariate space. Suppose a tree U has B terminal nodes. The corresponding piecewise stationary approximation is

$$X_{\ell t} \approx \sum_{b=1}^B \delta(\boldsymbol{\omega}_\ell; U, b) X_t^{(b)} = \int_{-1/2}^{1/2} \sum_{b=1}^B \delta(\boldsymbol{\omega}_\ell; U, b) A_b(\nu) \exp(2\pi i t \nu) dZ_\ell(\nu),$$

where $X_t^{(b)}$ is stationary process with power spectrum $f_b(\nu) = |A_b(\nu)|^2$ corresponding to the b th terminal node, and δ is a function that identifies terminal node membership for each observation based on covariates such that $\delta(\boldsymbol{\omega}_\ell; U, b) = 1$ if the ℓ th observation falls into the b th terminal node and $\delta(\boldsymbol{\omega}_\ell; U, b) = 0$ otherwise.

3.2 Local Power Spectrum Estimation

We now introduce an estimator for local power spectra within terminal nodes of the tree. Let $N = \lfloor T/2 \rfloor - 1$ and $\nu_k = k/T$ for $k = 1, \dots, N$ be the Fourier frequencies. The periodogram estimator of the power spectrum for the ℓ th time series is $I_\ell(\nu_k) = \frac{1}{T} \left| \sum_{t=1}^T X_{\ell t} \exp(-2\pi i \nu_k t) \right|^2$. The Whittle likelihood (Whittle, 1952), derived from the large sample distribution of the periodogram, can then be used to approximate the overall likelihood for the tree as a product of individual likelihoods, assuming T is sufficiently large,

$$L(I_1, \dots, I_\ell | f_1, \dots, f_B) \approx \prod_{\ell=1}^L \prod_{b=1}^B (2\pi)^{-N/2} \prod_{k=1}^N \exp\{-\delta(\boldsymbol{\omega}_\ell; U, b) [\log f_b(\nu_k) + \exp(\log I_\ell(\nu_k) - \log f_b(\nu_k))]\}. \quad (1)$$

Log power spectra within each terminal node $\log f_b(\nu)$ are modeled using a Bayesian penalized linear spline model (Rosen et al., 2012)

$$\log f_b(\nu) \approx \alpha_b + \sum_{s=1}^S \beta_s^{(b)} \cos(2\pi s \nu), \quad (2)$$

where the functions $\cos(2\pi s \nu)$ are the Demmler–Reinsch basis functions for periodic even splines observed on an evenly spaced grid (i.e. the Fourier frequencies) (Schwarz and Krivobokova, 2016, Section 3). Only the first $S < N$ basis functions are used to provide a low-rank approximation to the full linear smoothing spline (Eubank, 1999). In order to achieve good computational efficiency without sacrificing estimation accuracy (Krafty et al., 2017), $S = 7$

basis functions are used for subsequent simulations and real data analyses, which provide good empirical performance. Gaussian priors are assumed such that $\alpha_b \sim N(0, \sigma_\alpha^2)$ where σ_α^2 is a large constant value, and $\boldsymbol{\beta}^{(b)} = (\beta_1^{(b)}, \dots, \beta_S^{(b)})' \sim N(0, \tau_b^2 \mathbf{D}_S)$, where $\mathbf{D}_S = \text{diag}(\{\sqrt{2\pi}s\}^{-2})$. τ_b^2 is a smoothing parameter that controls the roughness of the log spectrum. The scaling for the smoothing parameter, $\{\sqrt{2\pi}s\}^{-2}$, provides regularization of the integrated squared first derivative of the log power spectrum (Li and Krafty, 2019). A half-t prior is placed on τ_b (Gelman, 2006) to complete the Bayesian model specification. We follow Wand et al. (2011) and express the half-t distribution as a scale mixture of inverse gamma distributions for efficient sampling. A two-step MCMC sampling scheme for α_b , $\boldsymbol{\beta}^{(b)}$, and τ_b following Rosen et al. (2012) is presented below.

- (1) Let \mathbf{Z}_b be a $N \times S$ matrix of basis functions for b th terminal node such that $\{Z_b\}_{k,s} = \cos(2\pi s\nu_k)$. Given τ_b , basis functions \mathbf{Z}_b , and periodogram ordinates $\mathbf{I}_\ell(\nu) = \{I_\ell(\nu_1), I_\ell(\nu_2), \dots, I_\ell(\nu_N)\}$ for $l = 1, \dots, L$, α_b and $\boldsymbol{\beta}^{(b)}$ are sampled jointly in a Metropolis-Hastings (M-H) step from

$$p(\alpha_b, \boldsymbol{\beta}^{(b)} | \tau_b^2, \mathbf{I}_\ell(\nu), \mathbf{Z}_b) \propto \exp \left\{ - \sum_{\ell=1}^L \sum_{k=1}^N [\alpha_b + \mathbf{z}'_{bk} \boldsymbol{\beta}^{(b)} + \exp(\log I_\ell(\nu_k) - \alpha_b - \mathbf{z}'_{bk} \boldsymbol{\beta}^{(b)})] - \frac{\alpha_b}{2\sigma_\alpha^2} - \frac{1}{2\tau_b^2} \boldsymbol{\beta}^{(b)'} \mathbf{D}_S^{-1} \boldsymbol{\beta}^{(b)} \right\}. \quad (3)$$

- (2) By representing the half-t prior as a scale mixture of inverse gamma distributions (Wand et al., 2011), we obtain draws of τ_b from its full conditional distribution by sampling from

$$(a_b | \tau_b^2) \sim \text{IG} \left(\frac{\xi_\tau + 1}{2}, \frac{\xi_\tau}{\tau_b^2} + \frac{1}{A_\tau^2} \right), \quad (4)$$

and

$$(\tau_b^2 | a_b, \boldsymbol{\beta}^{(b)}) \sim \text{IG} \left(\frac{\xi_\tau + S + 1}{2}, \frac{\boldsymbol{\beta}^{(b)'} \boldsymbol{\beta}^{(b)}}{2} + \frac{\xi_\tau}{a_b} \right) \quad (5)$$

where a_b is a latent variable, and ξ_τ and A_τ^2 are fixed hyperparameters of the inverse gamma distribution.

4. Adaptive Bayesian Sum of Trees Model

4.1 Sum of Trees Model

Poor mixing of single tree models has been noted in many applications such that the MCMC algorithm becomes stuck in subsets of the covariate space representing local optima and cannot efficiently traverse the entire parameter space (Wu et al., 2007). This can happen when single tree models grow very large in an effort to approximate more complex relationships, thus restricting possible modifications due to low sample size and an abundance of other splits. We follow Chipman et al. (2010) in developing a Bayesian sum of trees formulation to relieve this problem by constructing many shallow trees as “weak learners” for estimation.

Let M be the number of trees. A sum of trees model for the log power spectrum is then constructed as

$$\log f(\boldsymbol{\omega}, \nu) \approx \sum_{j=1}^M \sum_{b=1}^{B_j} \delta(\boldsymbol{\omega}; U_j, b) \log f_{bj}(\nu),$$

where U_j represents the j th tree that has B_j terminal nodes for $j = 1, \dots, M$. Model specification for local power spectra $\log f_{bj}(\nu)$ within each tree then follows directly from the specification for the single tree model introduced in Section 3.2.

4.2 Prior Specification

Let $\Phi_j = \{\log f_{1j}(\nu), \dots, \log f_{B_j j}(\nu)\}$ be the collection of log power spectra across terminal nodes for the j th tree. To complete the Bayesian model specification, priors are imposed on U_j and Φ_j in order to allow the trees to be random and fit from the data. Assuming independence across terminal node parameters and trees a priori, priors can be specified as

$$p((U_1, \Phi_1), \dots, (U_M, \Phi_M)) = \prod_j p(U_j, \Phi_j) = \prod_j p(\Phi_j | U_j) p(U_j),$$

where

$$p(\Phi_j | U_j) = \prod_b p(\log f_{bj}(\nu) | U_j).$$

The priors for $\Phi_j|U_j$ then correspond to the priors of α_b , $\beta^{(b)}$ and τ_b for the local power spectrum estimator introduced in Section 3.2. For the priors on the tree structure U_j , three probabilities need to be considered.

- (1) The probability of a node to be split is defined as $\Pr(\text{SPLIT}) = \gamma(1 + d)^{-\theta}$, where $\gamma \in (0, 1)$, $\theta \in [0, \infty)$ and $d = 0, 1, \dots$ is the depth of a given node. This prior is a regularization of the tree depth to encourage each tree to be shallow. We set $\gamma = 0.95$ and $\theta = 2$ following Chipman et al. (2010). Ročková and Saha (2019) propose a minor modification $\Pr(\text{SPLIT}) \propto \gamma^d$ for some $0 \leq \gamma < 1/2$ to achieve the optimal posterior convergence rate, which can also be adopted within the proposed framework.
- (2) The probability of selecting the p th covariate for splitting is denoted as s_p for $p = 1, \dots, P$. The proposed model allows for two possible prior specifications: a uniform prior, $s_p = P^{-1}$, such that all covariates have the same probability to be selected, and a sparsity-inducing Dirichlet prior $(s_1, \dots, s_P) \sim \mathcal{D}\left(\frac{\sigma}{P}, \dots, \frac{\sigma}{P}\right)$ (Lineró, 2018). For the Dirichlet prior, σ determines the degree of sparsity and Linero (2018) offer multiple approaches for modeling this parameter. We set $\sigma = 1$ as suggested by Linero (2018) for computational convenience.
- (3) The probability of selecting a particular cutpoint for a given covariate is uniform across all cutpoints. A uniform prior is also desirable as it is invariant for monotone transformations of the covariate (Chipman et al., 2010). For continuous, discrete, and ordinal covariates, cutpoints are selected from a fixed number of evenly spaced points over the range of possible values. For categorical covariates without an intrinsic ordering, a cutpoint represents a particular mapping of categories to the left and right child nodes created by the split. A categorical variable with q categories then has $2^q - 2$ cutpoints that can be selected.

4.3 Bayesian Backfitting MCMC

It is important to note that each tree is capturing particular features of the covariate-dependent power spectrum and also depends on the features captured by other trees. While this provides considerable flexibility and adaptive estimation, it presents significant computational challenges in estimating the trees. Following Chipman et al. (2010), we develop a Bayesian backfitting MCMC algorithm for proposing and evaluating modifications to each tree sequentially.

For the j th tree, the posterior distribution $p((U_1, \Phi_1), \dots, (U_M, \Phi_M) | \mathbf{I}_1(\nu_k), \dots, \mathbf{I}_L(\nu_k))$ can be sampled through M successive draws from $p((U_j, \Phi_j) | U_{-j}, \Phi_{-j}, \mathbf{I}_1(\nu_k), \dots, \mathbf{I}_L(\nu_k))$ where U_{-j} is the set of all trees except U_j , and Φ_{-j} is defined similarly. Observe that the conditional distribution $p((U_j, \Phi_j) | U_{-j}, \Phi_{-j}, \mathbf{I}_1(\nu_k), \dots, \mathbf{I}_L(\nu_k))$ depends on $(U_{-j}, \Phi_{-j}, \mathbf{I}_1(\nu_k), \mathbf{I}_2(\nu_k), \dots, \mathbf{I}_L(\nu_k))$ only through

$$\mathbf{R}_{\ell_j}(\nu_k) = \log \mathbf{I}_{\ell}(\nu_k) - \sum_{i \neq j} \sum_{b=1}^{B_j} \delta(\boldsymbol{\omega}; U_i, b) \log f_{bi}(\nu),$$

where $\mathbf{R}_{\ell_j}(\nu_k)$ is the residual of the log periodogram after removing the fit from the sum of trees across all trees except for the j th tree. Therefore, drawing from the posterior distribution equates to M successive draws from $p((U_j, \Phi_j) | \mathbf{R}_{1j}(\nu_k), \dots, \mathbf{R}_{Lj}(\nu_k))$. Hence, the local power spectrum estimator for the j th tree is then fit by replacing $\log \mathbf{I}_{\ell}(\nu_k)$ with $\mathbf{R}_{\ell_j}(\nu_k)$ in Equation (1) and Equation (3).

4.4 Reversible-jump MCMC Sampling

To sample new tree structures, a reversible-jump MCMC (RJ-MCMC) (Green, 1995) procedure is developed to jointly propose and evaluate new draws of U and Φ for each tree. The proposed modification takes the form of one of three possible moves: BIRTH, DEATH and CHANGE, with probabilities 0.25, 0.25 and 0.5 respectively. The BIRTH move grows the tree by splitting a terminal node into two child nodes, the DEATH move prunes the tree by dropping two terminal child nodes belonging to the same internal node, and the CHANGE

move modifies the variable and cut point associated with an internal node with two terminal child nodes. New model parameters for the proposed tree modification are drawn, and the proposed tree modification is then accepted or rejected using a Metropolis–Hastings (M-H) step. Each tree is considered in turn for updating within each iteration. Draws using this RJMCMC sampling scheme are repeated and averaged over post burn-in draws to obtain the final estimator. Technical details for the RJMCMC sampling scheme are available in Web Appendix A.

5. Simulation Studies

We consider three simulation settings representing abrupt and smoothly varying dynamics with complex covariate effects and interactions in order to demonstrate strong finite-sample estimation accuracy, as well as the ability to adapt to sparse covariate effects and conduct variable selection.

5.1 Settings

- (1) Abrupt+Smooth: Let $\boldsymbol{\omega} = (\omega_1, \omega_2)$ where $\omega_1, \omega_2 \stackrel{i.i.d.}{\sim} U(0, 1)$. An AR(1) process for the ℓ th time series is specified as $x_{\ell t} = \phi_{\ell} x_{\ell t-1} + \epsilon_{\ell t}$, $\epsilon_{\ell t} \sim N(0, 1)$, where $\phi_{\ell} = -0.7 + 1.4\omega_2$ when $0 \leq \omega_1 < 0.5$ and $\phi_{\ell} = 0.9 - 1.8\omega_2$, when $0.5 \leq \omega_1 \leq 1$.
- (2) AR-Friedman: Let $\boldsymbol{\omega} = (\omega_1, \dots, \omega_5)$ where $\omega_1, \dots, \omega_5 \stackrel{i.i.d.}{\sim} U(0, 1)$. An AR(1) process for the ℓ th time series is specified as $x_{\ell t} = \phi_{\ell} x_{\ell t-1} + \epsilon_{\ell t}$, $\epsilon_{\ell t} \sim N(0, 1)$, where $\phi_{\ell} = 0.5 \sin(\pi\omega_{\ell 1}\omega_{\ell 2}) - (\omega_{\ell 3} - 0.5)^2 + 0.35\text{sign}(\omega_{\ell 4} - 0.5) - 0.15\omega_{\ell 5}$.
- (3) Adjusted-AdaptSPEC-X: Let $\boldsymbol{\omega} = (\omega_1, \omega_2)$, where $\omega_1, \omega_2 \stackrel{i.i.d.}{\sim} U(0, 1)$. Each covariate vector $\boldsymbol{\omega}$ is mapped to a latent variable $z_{\ell} \in \{1, 2, 3, 4\}$. Figure 6 shows the mapping from $\boldsymbol{\omega}$ to z . An AR(2) process is then specified as $x_{\ell t} = \phi_{z_{\ell} 1} x_{\ell t-1} + \phi_{z_{\ell} 2} x_{\ell t-2} + \epsilon_{\ell t}$, $\epsilon_{\ell t} \sim N(0, 1)$, where the coefficients for the four latent region are defined as follows. If $z_{\ell} = 1$,

$(\phi_{z_\ell 1}, \phi_{z_\ell 2}) = (1.5, -0.75)$; if $z_\ell = 2$, $(\phi_{z_\ell 1}, \phi_{z_\ell 2}) = (-0.8, 0)$; if $z_\ell = 3$, $(\phi_{z_\ell 1}, \phi_{z_\ell 2}) = (-1.5, -0.75)$; if $z_\ell = 4$, $(\phi_{z_\ell 1}, \phi_{z_\ell 2}) = (0.2, 0)$.

[Figure 2 about here.]

The first setting represents an AR(1) process in which the coefficient varies smoothly across one covariate and abruptly across another. The second setting contains complex linear and nonlinear covariate effects and interactions (Friedman, 1991) adapted for time series data. The third setting represents an abruptly-changing process over two dimensions, similar to that of Bertolacci et al. (2019).

5.2 Results: Estimation Accuracy

Hyperparameters are specified as $\sigma_\alpha^2 = 100$ for the prior variance of α_b in Equation (2) and $\xi_\tau = 2$ and $A_\tau = 10$ for the prior on τ_b in Equation (4) and Equation (5). We used $M = 5$ trees for estimation, and different numbers (L) and lengths (T) of time series are considered. The MCMC procedure is run for a total of 10,000 iterations with the first 5,000 discarded as burn-in. In order to assess convergence, trace plots for summary measures of the mean squared residuals, estimated log power spectrum, and tree structures for all settings are available in the Web Appendix B. These diagnostics appear to show convergence after approximately 5,000 iterations across all settings.

Estimates of the covariate-dependent power spectrum for this run are presented in Figure 3 to visually illustrate the ability of the proposed method to capture abrupt and smooth changes in power spectra. The smooth change in the conditional power spectrum over ω_2 is captured by averaging over the posterior distribution of tree structures, which contains many splits across the range of possible values of ω_2 . On the other hand, splits on ω_1 are concentrated around the true abrupt change at $\omega_1 = 0.5$, and the posterior mean estimator of the conditional power spectrum over ω_1 appropriately reflects the abrupt change in the conditional power spectrum.

[Figure 3 about here.]

To evaluate estimation accuracy, the mean and standard deviation of the mean squared error (MSE) is presented in Table 1 for 100 replications of all settings. For comparison, AdaptSPEC-X (Bertolacci et al., 2019) is also used to estimate the covariate-dependent power spectrum. It is important to note that AdaptSPEC-X allows for modeling of time- and covariate-varying power spectra with time-varying means, which is a more general setting than what is considered in this work. Accordingly, we implement a simplified version of the AdaptSPEC-X mixture model without the time-varying mean and power spectra components to enable more accurate comparisons. We applied $C = 50$ mixture components to ensure sufficient flexibility in estimating covariate effects on power spectra.

[Table 1 about here.]

These results show that both methods see improved estimation accuracy as the number (L) and length (T) of time series increase. However, the proposed method generally carries smaller MSEs than AdaptSPEC-X for comparable settings. This can be partially attributed to the presence of abrupt changes across one or more covariates in all settings, which are better captured by the proposed tree-based approach. To illustrate this point, Figure 2(b) shows the estimated power spectra for two simulated time series with similar covariate values separated by an abrupt change from the Adjusted-AdaptSPEC-X setting. As noted in Bertolacci et al. (2019), the thin-plate Gaussian process prior on the mixture weights, while flexible, is both smooth and stationary. Accordingly, the AdaptSPEC-X power spectrum estimates for these two time series are similar due to smoothing across similar covariate values induced by the thin-plate Gaussian process prior. On the other hand, the proposed Bayesian sum-of-trees model is able to accurately distinguish the abrupt change in the power spectra. Moreover, averaging over the posterior distribution of trees enables the proposed

method to recover smooth changes well (Figure 3). Taken together, this results in superior estimation accuracy across all settings seen in Table 1.

5.3 Results: Computation Time

Simulations were carried out on a Windows 10 machine with an 8-core Intel i7 3.6 GHz processor and 64 GB RAM using R version 4.0.3 (R Core Team, 2021). The R code for implementing the proposed model is provided as a zip file in Supporting Information and is described in Web Appendix C. Computationally-intensive aspects of the methodology are written in C++ using `RcppArmadillo` (Eddelbuettel and Sanderson, 2014) for more efficient computation and reduced run times. Replications were run in parallel across six cores. For the simulation settings considered herein, the mean run time for each tree update after burn-in ranges from 0.02 to 0.43 seconds, depending on the number (L) and length (T) of time series. The distribution of mean run times for each setting with different L and T and $M = 5$ trees are visualized in the Web Appendix B.

While run times generally increase as the number and length of time series increase, length increases have a bigger impact on run times relative to increases in the number of time series. Increasing T from 100 to 500 while holding L constant increases mean run times by a multiple of approximately 3.5, while increasing L from 100 to 500 while holding T constant increases mean run times by a multiple of approximately 2.1. This is expected since the number of Fourier frequencies grows with the length of the series and increases both the number of terms being summed in the log Whittle likelihood and the dimension of the cosine basis used to approximate local log power spectra. However, increasing the number of time series does not change the number of Fourier frequencies and only requires adding more terms in the log Whittle likelihood and posterior distribution for the spline coefficients, which is less computationally expensive. See Equations (1)-(3) in Section 3.2 and sampling scheme details in the Web Appendix A for more details.

Tree size also plays an important role in determining run times for tree updates. Larger trees tend to have fewer time series belonging to each terminal node, which reduces computational burden and run times for evaluating modifications to a single terminal node. This is why the Adjusted-AdaptSPEC-X setting, which requires larger trees to recover the complex covariate effects, has faster mean run times compared to other settings. Additionally, tree size tends to increase as both L and T increase. For illustration, the Web Appendix B includes a plot of the total number of bottom nodes for different combinations of L and T for the AR-Friedman simulation setting. This can also help explain why run times grow more slowly in L compared to T .

5.4 Results: Sparse Covariate Effects

In order to demonstrate the capability of the proposed method in providing efficient variable selection by adapting to sparse covariate effects for high-dimensional covariates, we consider a modification to the AR-Friedman simulation setting introduced previously. The original covariate vector containing 5 important covariates is now extended to include 95 additional noise covariates independently drawn from a standard normal distribution. Variable selection efficiency can be investigated by assessing the estimated posterior probability for model inclusion of each covariate, which is the proportion of posterior draws where the covariate appears in at least one split rule for at least one tree. The estimated posterior probabilities for model inclusion for each of the 100 covariates using the uniform hyperprior and the sparsity-inducing Dirichlet prior for a single run of the proposed algorithm are shown in Web Appendix B. Both forms of the prior correctly estimate the posterior probabilities of model inclusion to be 1 for all 5 important variables, but the Dirichlet prior accurately achieves a sparser solution with the posterior probability of inclusion for the noise variables being much closer to 0. Specifically, the mean posterior probability of inclusion for noise variables using the uniform prior is 0.11 with a standard deviation of 0.1861, and the mean

posterior probability of inclusion for noise variables using the Dirichlet prior is 0.01 with a standard deviation of 0.1026. For high-dimensional covariates in which only a few covariates are expected to be associated with the properties of the time series, the Dirichlet prior provides accurate selection of important covariates.

6. Gait Maturation Analysis

We now present the analytical results of applying the proposed method to the motivating gait maturation study described in the introduction (Goldberger et al., 2000). The current analysis considers the effect of age on gait variability to better understand gait maturation in young children in the presence of other factors that may influence gait, such as gender and gait speed. The data contains stride interval time series from 50 healthy children with equal numbers of girls and boys between 3 and 14 years old. The time series consist of $T = 256$ stride times during normal walking after removing the first 60 seconds and last 5 seconds to avoid warm-up and ending effects (Figure 1). More details of data processing can be found in Hausdorff et al. (1999). The proposed Bayesian sum of trees model was used to estimate the covariate-dependent power spectrum of stride interval time series using 5 trees and 10,000 total iterations with the first 5,000 iterations discarded as burn-in. See Web Appendix B for convergence diagnostics of this application.

Partial dependence (PD) (Friedman, 2001) is the most widely used method for evaluating covariate effects in machine learning models. However, there is an issue with multicollinearity in this dataset, as age and gait speed are significantly correlated ($r = 0.653, p < 0.0001$), which can render PD unreliable due to extrapolation of the response at predictor values far outside the multivariate envelope of the data (Apley and Zhu, 2020). Therefore, we use accumulated local effects (ALE) (Apley and Zhu, 2020) to characterize covariate effects. ALE presents the effect in a small interval of the interested feature, which can mitigate issues with multicollinearity by localizing the estimated effect within the envelope of the

data. Let $\boldsymbol{\omega} = (\omega_j, \boldsymbol{\omega}_{\setminus j})$ where ω_j denotes the j th covariate and $\boldsymbol{\omega}_{\setminus j}$ denotes all covariates other than the j th covariate. The ALE for $\omega_j = x$ on the power spectrum at frequency ν is defined as

$$f_{j,\text{ALE}}(x, \nu) = \int_{z_{0,j}}^x E_{\boldsymbol{\omega}_{\setminus j} | \omega_j} \left[\frac{\delta f(\boldsymbol{\omega}, \nu)}{\delta \omega_j} \Big|_{\omega_j = z_j} \right] dz_j - \text{constant} \quad (6)$$

where $\mathbb{Z}_j = \{z_{0,j}, \dots, z_{H,j}\}$ is a collection of $H + 1$ partition points over the effective support of ω_j . The constant is a value to vertically center the plot. Let $\hat{f}(z_{h,j}, x_{\setminus j}; \nu)$ be the estimated power spectrum for $\omega_j = z_{h,j}$, $h = 1, \dots, H$ and $\boldsymbol{\omega}_{\setminus j} = x_{\setminus j}$ on frequency ν , the uncentered ALE can then be estimated by

$$\hat{g}_{j,\text{ALE}}(x, \nu) = \sum_{h=1}^{h_j(x)} \frac{1}{n_j(h)} \sum_{\{i: x_j^{(i)} \in N_j(h)\}} \left[\hat{f}(z_{h,j}, x_{\setminus j}^{(i)}; \nu) - \hat{f}(z_{h-1,j}, x_{\setminus j}^{(i)}; \nu) \right] \quad (7)$$

where $h_j(x)$ is the index for the interval of the partition \mathbb{Z}_j to which the value x belongs, n is the total number of observations and $n_j(h)$ is the number of observations in the h th segment of the partition for ω_j such that $\sum_{h=1}^H n_j(h) = n$. $N_j(h) = (z_{h-1,j}, z_{h,j}]$ represents the h th interval of the partition for ω_j . Then the estimated centered ALE is

$$\hat{f}_{j,\text{ALE}}(x, \nu) = \hat{g}_{j,\text{ALE}}(x, \nu) - \frac{1}{n} \sum_{i=1}^n \hat{g}_{j,\text{ALE}}(x^{(i)}, \nu). \quad (8)$$

By partitioning covariates into $H = 5$ intervals containing equal numbers of observations, Figures 4(a) and 4(b) show the posterior mean of the ALE for age and gait speed on the power spectrum. Two findings can be concluded from these plots. First, power over all frequencies decreases as age increases. This indicates variability in stride times decreases with age, which is consistent with previous findings (Hausdorff et al., 1999). Second, we can observe that power in low frequencies (LF) (0.05-0.25 stride⁻¹) decreases much more with age relative to higher frequencies (HF) (0.25-0.5 stride⁻¹). This is also expected as low frequency power corresponds to fluctuations over relatively longer time scales and is indicative of less mature neuromuscular control (Hausdorff et al., 1999). To further illustrate this point, Figures 4(c)

and 4(d) present the posterior mean of the ALE of age and gait speed on the LF/HF ratio

$$\frac{\text{LF}}{\text{HF}}(\boldsymbol{\omega}) = \frac{\int_{0.05}^{0.25} f(\boldsymbol{\omega}, \nu) d\nu}{\int_{0.25}^{0.5} f(\boldsymbol{\omega}, \nu) d\nu}$$

along with 95% pointwise credible intervals. This can be computed by replacing the power spectrum $f(\boldsymbol{\omega}, \nu)$ and estimated power spectrum $\hat{f}(z_{h,j}, x_{\setminus j}; \nu)$ in Equations (6)-(8) with the $\frac{\text{LF}}{\text{HF}}(\boldsymbol{\omega})$ and its corresponding estimates

$$\frac{\widehat{\text{LF}}}{\widehat{\text{HF}}}(\boldsymbol{\omega}) = \frac{\sum_{\nu_k \in (0.05, 0.25)} \hat{f}(\boldsymbol{\omega}, \nu_k)}{\sum_{\nu_k \in (0.25, 0.5)} \hat{f}(\boldsymbol{\omega}, \nu_k)}$$

where $\frac{\widehat{\text{LF}}}{\widehat{\text{HF}}}(\boldsymbol{\omega})$ can be expressed as $\frac{\widehat{\text{LF}}}{\widehat{\text{HF}}}(z_{h,j}, x_{\setminus j})$ when calculating the ALE for the j th covariate.

While LF/HF($\boldsymbol{\omega}$) decreases significantly with both age and gait speed, we see relatively larger decreases beyond 7 years of age and for speeds above 1 m/sec. This is also consistent with previous findings (Hausdorff et al., 1999), showing the LF/HF ratio does not show a significant decrease in children 3-7 years of age, but does show a significant decrease in children 7-14 years of age. Noting that gait speed is positively correlated with age, it is expected that speed exhibits similar association with the power spectrum. Our analysis (not shown) did not indicate a significant gender effect on either the stride interval power spectrum or LF/HF ratio.

[Figure 4 about here.]

7. Discussion

This paper describes a novel adaptive Bayesian covariate-dependent model for the power spectrum of multiple time series. By using a sum of trees model to characterize covariate effects, this model is flexible and can automatically recover complex nonlinear associations and interactions as well as provide efficient variable selection.

This article is one of the first approaches to analyzing the power spectrum of multiple stationary time series with multiple covariates in a completely nonparametric manner, but it is not without limitations. An important direction for future research is to extend the

proposed Bayesian sum of trees model to accommodate additional data features commonly encountered in practice, such as time- and covariate-dependent time series (Bertolacci et al., 2019), extra spectral variability due to clustering effects (Krafty, 2016), and missingness in covariate vectors. Alternative partitioning frameworks, such as Voronoi tessellations (Payne et al., 2020) and binary space partitioning trees (Fan et al., 2019), may also be considered for capturing covariate effects in an even more flexible and parsimonious manner.

Acknowledgements

This work is supported by the National Institute of General Medical Sciences of the National Institutes of Health under Award Number R01GM140476.

References

- Adak, S. (1998). Time-dependent spectral analysis of nonstationary time series. *Journal of the American Statistical Association* **93**, pp. 1488-1501.
- Apley, D. W. and Zhu, J. (2020). Visualizing the effects of predictor variables in black box supervised learning models. *Journal of the Royal Statistical Society. Series B, Statistical Methodology* **82**, 1059–1086.
- Bertolacci, M., Rosen, O., Cripps, E., and Cripps, S. (2019). AdaptSPEC-X: Covariate dependent spectral modeling of multiple nonstationary time series. *ArXiv* .
- Blattenberger, G. and Fowles, R. (2017). Treed avalanche forecasting: Mitigating avalanche danger utilizing Bayesian additive regression trees. *Journal of Forecasting* **36**, 165–180.
- Breiman, L. (2001). Random forests. *Machine Learning* **45**, 5–32.
- Brenière, Y. and Bril, B. (1988). Why do children walk when falling down while adults fall down in walking? *Comptes Rendus de l'Académie des Sciences. Série III, Sciences de la Vie* **307**, 617–22.
- Brillinger, D. R. (2002). *Time Series: Data Analysis and Theory*. Philadelphia: SIAM.

- Bruce, S. A., Hall, M. H., Buysse, D. J., and Krafty, R. T. (2018). Conditional adaptive Bayesian spectral analysis of nonstationary biomedical time series. *Biometrics* **74**, 260–269.
- Chau, J. and von Sachs, R. (2016). Functional mixed effects wavelet estimation for spectra of replicated time series. *Electronic Journal of Statistics* **10**, 2461 – 2510.
- Chipman, H., George, E. I., Gramacy, R. B., and McCulloch, R. (2013). Bayesian treed response surface models. *WIREs Data Mining and Knowledge Discovery* **3**, 298–305.
- Chipman, H. A., George, E. I., and McCulloch, R. E. (2010). BART: Bayesian additive regression trees. *The Annals of Applied Statistics* **4**, 266–298.
- Cramér, H. (1942). On harmonic analysis in certain function spaces. *Arkiv för Matematik, Astronomioch Fysik* **28B**, 1–7.
- Diggle, P. J. and Al Wasel, I. (1997). Spectral analysis of replicated biomedical time series. *Journal of the Royal Statistical Society: Series C (Applied Statistics)* **46**, 31–71.
- Eddelbuettel, D. and Sanderson, C. (2014). RcppArmadillo: Accelerating R with high-performance C++ linear algebra. *Computational Statistics and Data Analysis* **71**, 1054–1063.
- Eubank, R. (1999). *Nonparametric Regression and Spline Smoothing*. Boca Raton: CRC Press.
- Fan, X., Li, B., and Sisson, S. (2019). Binary space partitioning forest. In *The 22nd International Conference on Artificial Intelligence and Statistics*, pages 3022–3031. PMLR.
- Fiecas, M. and Ombao, H. (2017). Modeling the evolution of dynamic brain processes during an associative learning experiment. *Journal of the American Statistical Association* **111**, 1440–1453.
- Friedman, J. H. (1991). Multivariate adaptive regression splines. *The Annals of Statistics*

19, 1–67.

- Friedman, J. H. (2001). Greedy function approximation: A gradient boosting machine. *The Annals of Statistics* **29**, 1189–1232.
- Gelman, A. (2006). Prior distributions for variance parameters in hierarchical models (comment on article by Browne and Draper). *Bayesian Anal.* **1**, 515–534.
- Goldberger, A. L., Amaral, L. A. N., Glass, L., Hausdorff, J. M., Ivanov, P. C., Mark, R. G., Mietus, J. E., Moody, G. B., Peng, C.-K., and Stanley, H. E. (2000). PhysioBank, PhysioToolkit, and PhysioNet: Components of a new research resource for complex physiologic signals. *Circulation* **101**, 215–220.
- Green, P. J. (1995). Reversible jump markov chain monte carlo computation and Bayesian model determination. *Biometrika* **82**, 711–732.
- Hall, M., Vasko, R., Buysse, D., Ombao, H., Chen, Q., Cashmere, J. D., Kupfer, D., and Thayer, J. F. (2004). Acute stress affects heart rate variability during sleep. *Psychosomatic Medicine* **66**, 56-62.
- Hausdorff, J. M., Zemani, L., Peng, C.-K., and Goldberger, A. L. (1999). Maturation of gait dynamics: Stride-to-stride variability and its temporal organization in children. *Journal of Applied Physiology* **86**, 1040–1047.
- Iannaccone, R. and Coles, S. (2001). Semiparametric models and inference for biomedical time series with extra-variation. *Biostatistics* **2**, 261–276.
- Klimesch, W. (1999). EEG alpha and theta oscillations reflect cognitive and memory performance: A review and analysis. *Brain Research Reviews* **29**, 169-195.
- Krafty, R. T. (2016). Discriminant analysis of time series in the presence of within-group spectral variability. *Journal of Time Series Analysis* **37**, 435–450.
- Krafty, R. T., Hall, M., and Guo, W. (2011). Functional mixed effects spectral analysis. *Biometrika* **98**, 583–598.

- Krafty, R. T., Rosen, O., Stoffer, D. S., Buysse, D. J., and Hall, M. H. (2017). Conditional spectral analysis of replicated multiple time series with application to nocturnal physiology. *Journal of the American Statistical Association* **112**, 1405–1216.
- Li, Z., Bruce, S. A., Wutzke, C. J., and Long, Y. (2021). Conditional adaptive Bayesian spectral analysis of replicated multivariate time series. *Statistics in Medicine* **40**, 1989–2005.
- Li, Z. and Krafty, R. T. (2019). Adaptive Bayesian time-frequency analysis of multivariate time series. *Journal of the American Statistical Association* **114**, 453–465.
- Linero, A. R. (2018). Bayesian regression trees for high-dimensional prediction and variable selection. *Journal of the American Statistical Association* **113**, 626–636.
- Payne, R. D., Guha, N., Ding, Y., and Mallick, B. K. (2020). A conditional density estimation partition model using logistic gaussian processes. *Biometrika* **107**, 173–190.
- Preis, S., Klemms, A., and Müller, K. (2008). Gait analysis by measuring ground reaction forces in children: Changes to an adaptive gait pattern between the ages of one and five years. *Developmental Medicine and Child Neurology* **39**, 228–233.
- Qin, L., Guo, W., and Litt, B. (2009). A time-frequency functional model for locally stationary time series data. *Journal of Computational and Graphical Statistics* **18**, 675–693.
- R Core Team (2021). *R: A Language and Environment for Statistical Computing*. R Foundation for Statistical Computing, Vienna, Austria.
- Rosen, O., Wood, S., and Stoffer, D. (2012). AdaptSPEC: Adaptive spectral estimation for nonstationary time series. *Journal of the American Statistical Association* **107**, 1575–1589.
- Ročková, V. and Saha, E. (2019). On theory for BART. In *Proceedings of Machine Learning Research*, volume 89 of *Proceedings of Machine Learning Research*, pages 2839–2848.

PMLR.

Schwarz, K. and Krivobokova, T. (2016). A unified framework for spline estimators.

Biometrika **103**, 121–131.

Shumway-Cook, A. and Williams, M. W. (1995). Motor control: Theory and practical applications.

Starling, J. E., Murray, J. S., Carvalho, C. M., Bukowski, R. K., Scott, J. G., et al. (2020).

BART with targeted smoothing: An analysis of patient-specific stillbirth risk. *Annals of Applied Statistics* **14**, 28–50.

Stoffer, D. S., Han, S., Qin, L., and Guo, W. (2010). Smoothing spline ANOPOW. *Journal of Statistical Planning and Inference* **140**, 3789–3796.

van der Merwe, S. (2018). Time series analysis of the southern oscillation index using Bayesian additive regression trees. *ArXiv*.

Waldmann, P. (2016). Genome-wide prediction using Bayesian additive regression trees. *Genetics Selection Evolution (Paris)* **48**, 42–.

Wand, M. P., Ormerod, J. T., Padoan, S. A., and Frühwirth, R. (2011). Mean field variational Bayes for elaborate distributions. *Bayesian Anal.* **6**, 847–900.

Whittle, P. (1952). The simultaneous estimation of a time series harmonic components and covariance structure. *Trabajos de Estadística* **3**, 43-57.

Wu, Y., Tjelmeland, H., and West, M. (2007). Bayesian CART: Prior specification and posterior simulation. *Journal of Computational and Graphical Statistics* **16**, 44–66.

Web Appendix A: Sampling Scheme Details

The sampling scheme for the proposed Bayesian sum of trees model for the covariate-dependent power spectrum is presented in this section. Suppose we have M trees for the sum of trees model. Let (U_j, Φ_j) and (U_j^*, Φ_j^*) be the current and proposed tree structure and terminal node parameter estimates respectively for the j th tree, and let \mathbf{R}_j denote the residuals of the log periodogram ordinates from the fit corresponding to the sum of all trees except the j th tree for all time series. More details about the types of proposals developed in this work are provided herein. For ease of exposition, the subscript j is dropped in what follows. We implement the reversible jump Markov chain Monte Carlo (MCMC) sampling scheme by using a Metropolis-Hastings algorithm in which the acceptance ratio α is formulated as

$$\alpha = \min\{1, A\},$$

where

$$A = \frac{p(U^*, \Phi^* | \mathbf{R}) \times q(U, \Phi | U^*, \Phi^*)}{p(U, \Phi | \mathbf{R}) \times q(U^*, \Phi^* | U, \Phi)}.$$

More details on the individual components of the acceptance ratio introduced above are provided below.

i. Distribution of $p(U, \Phi | \mathbf{R})$ and $p(U^, \Phi^* | \mathbf{R})$* The joint posterior distribution $p(U, \Phi | \mathbf{R})$ can be expressed as a product of the following terms

$$\begin{aligned} p(U, \Phi | \mathbf{R}) &= p(\mathbf{R} | U, \Phi) \times p(\Phi | U) \times p(U) \\ &= p(\mathbf{R} | U, \Phi) \times p(\boldsymbol{\beta}, \tau^2 | U) \times p(U) \\ &= \underbrace{p(\mathbf{R} | U, \Phi)}_{\text{likelihood}} \times \underbrace{p(\boldsymbol{\beta} | U, \tau^2) \times p(\tau^2 | U)}_{\text{prior}} \times p(U), \end{aligned}$$

where the prior of Φ is determined by the joint prior of $(\boldsymbol{\beta}, \tau^2)$. Here, $\boldsymbol{\beta}$ represents the

intercept and basis coefficients in Equation (1) of the manuscript. Suppose there are n_b observations in the b th terminal node of j th tree for $b = 1, \dots, B$, the likelihood can be expressed as the product of individual Whittle likelihoods

$$p(\mathbf{R}|U, \Phi) = \prod_{b=1}^B p(\mathbf{R}_{b1}, \dots, \mathbf{R}_{bn_b} | f_{jb}) \approx \prod_{b=1}^B \prod_{i=1}^{n_b} (2\pi)^{-n/2} \prod_{k=1}^n \exp\{\log f_{jb}(\nu_k) + \exp(\mathbf{R}_{bi}(\nu_k)) / f_{jb}(\nu_k)\}, \quad (9)$$

where $n = \lfloor T/2 \rfloor - 1$, $\nu_k = k/T$ for $k = 1, \dots, n$ are the Fourier frequencies, T is the length of time series, and \mathbf{R}_{bi} is the residual of the log periodogram ordinates for the i th time series belonging to the b th terminal node.

The prior for β is a normal distribution such that $p(\beta|U, \tau^2) \sim N(0, (\sigma_\alpha^2, \tau^2 \mathbf{D}_S))$ as described in Section 3.2 of the manuscript. The prior distribution for τ^2 , $p(\tau^2|U)$, is a half-t distribution. We follow Wand et al. (2011) and express the half-t distribution as a scale mixture of inverse gamma distributions with latent variable a such that

$$p(\tau^2|a) \sim \text{IG}\left(\frac{\xi_\tau}{2}, \frac{\xi_\tau}{a}\right), \quad p(a) \sim \text{IG}\left(\frac{1}{2}, \frac{1}{A_\tau^2}\right).$$

The prior for the tree structure $p(U)$ is

$$p(U) = \prod_{\eta \in \text{terminals}} [1 - p_{\text{split}}(\eta)] \prod_{\eta \in \text{internals}} p_{\text{split}}(\eta) \prod_{\eta \in \text{internals}} p_{\text{rule}}(\eta),$$

where η is the node of the current tree. The $p_{\text{split}}(\eta) = \gamma(1+d)^{-\theta}$ is the probability of node η to be split into two child nodes with $\gamma \in (0, 1)$, $\theta \in [0, \infty)$ and $d = 0, 1, \dots$ which is the depth of the given node η . The $p_{\text{rule}}(\eta) = \frac{1}{n_{\text{adj}}(\eta)} \times \frac{1}{n_{\text{cutpoint}}(\eta)}$ is the probability of the available variables and the cutpoints to be chosen for node η , where $n_{\text{adj}}(\eta)$ denotes the number of predictors available for the node and $n_{\text{cutpoint}}(\eta)$ is the number of available cutpoints for the selected variable. The posterior distribution $p(U^*, \Phi^* | \mathbf{R})$ is similar with $p(U, \Phi | \mathbf{R})$ by plugging in U^* and Φ^* instead.

ii. *Distribution of $q(U^*, \Phi^*|U, \Phi)$ and $q(U, \Phi|U^*, \Phi^*)$* The proposed density $q(U^*, \Phi^*|U, \Phi)$

is defined as

$$\begin{aligned} q(U^*, \Phi^*|U, \Phi) &= q(\Phi^*|U^*, U, \Phi) \times q(U^*|U, \Phi) \\ &= q(\boldsymbol{\beta}^*, \tau^{2*}|U^*, U, \Phi) \times q(U^*|U) \\ &= q(\tau^{2*}|U^*, U, \Phi) \times q(\boldsymbol{\beta}^*|\tau^{2*}, U^*, U, \Phi) \times q(U^*|U), \end{aligned}$$

and similarly, the density $q(U, \Phi|U^*, \Phi^*)$ is

$$\begin{aligned} q(U, \Phi|U^*, \Phi^*) &= q(\Phi|U^*, \Phi^*, U) \times q(U|U^*, \Phi^*) \\ &= q(\boldsymbol{\beta}, \tau^2|U^*, \Phi^*, U) \times q(U|U^*) \\ &= q(\tau^2|U^*, \Phi^*, U) \times q(\boldsymbol{\beta}|\tau^2, U^*, \Phi^*, U) \times q(U|U^*). \end{aligned}$$

From part **i** and part **ii**, A can be written as

$$\underbrace{\frac{p(\mathbf{R}|U^*, \Phi^*)}{p(\mathbf{R}|U, \Phi)}}_{\text{likelihood ratio}} \times \underbrace{\frac{p(\boldsymbol{\beta}^*|U^*, \tau^{2*})p(\tau^{2*}|U^*)}{p(\boldsymbol{\beta}|U, \tau^2)p(\tau^2|U)}}_{\text{prior ratio}} \times \underbrace{\frac{p(U^*)}{p(U)}}_{\text{tree structure ratio}} \times \underbrace{\frac{q(\boldsymbol{\beta}, \tau^2|U^*, \Phi^*, U)}{q(\boldsymbol{\beta}^*, \tau^{2*}|U, \Phi, U^*)}}_{\text{proposed probability ratio}} \times \underbrace{\frac{q(U|U^*)}{q(U^*|U)}}_{\text{transition ratio}}. \quad (10)$$

Proposed modifications to the tree structures can take the form of one of three possible moves: BIRTH, DEATH and CHANGE. The BIRTH move grows the tree by splitting a terminal node into two child nodes, the DEATH move prunes the tree by dropping two terminal child nodes belonging to the same internal node, and the CHANGE move modifies the variable and cut point associated with an internal node with two terminal child nodes. Noticing that the prior ratio is the same for all BIRTH, DEATH, and CHANGE moves, the other ratios will be described individually for each of the three types of moves.

BIRTH

For the BIRTH move, the b th terminal node of the j th tree is selected to be split into two new child nodes. The proposed tree differs from the original tree only through the change

from this terminal node to new child nodes. Therefore, the likelihood ratio becomes

$$\frac{p(\mathbf{R}|U^*, \Phi^*)}{p(\mathbf{R}|U, \Phi)} = \frac{p(\mathbf{R}_{b_l1}, \dots, \mathbf{R}_{b_l n_l} | f_{j b_l}) p(\mathbf{R}_{b_r1}, \dots, \mathbf{R}_{b_r n_r} | f_{j b_r})}{p(\mathbf{R}_{b1}, \dots, \mathbf{R}_{b n_b} | f_{j b})},$$

where b_l denotes left child node, b_r is for the right child node, n_l is the number of series corresponding to the proposed left child node, n_r is the number of series corresponding to the proposed right child node, $\mathbf{R}_{b_l i}$ are residuals of the log periodogram ordinates for the i th series corresponding to the proposed left child node, and $\mathbf{R}_{b_r i}$ defined similarly for the proposed right child node. The likelihood within the terminal node is as shown in Equation (9). The tree structure ratio is expressed as

$$\frac{p(U^*)}{p(U)} = \frac{(1 - p_{\text{split}}(b_l))(1 - p_{\text{split}}(b_r))p_{\text{split}}(b)p_{\text{rule}}(b)}{1 - p_{\text{split}}(b)}.$$

For the transition probability $q(U|U^*)$ and $q(U^*|U)$, they can be expressed as

$$\begin{aligned} q(U^*|U) &= p(\text{GROW}) \times p(\text{selecting the } b\text{th terminal node to grow from}) \\ &\quad \times p(\text{selecting the } q\text{th predictor to split on}) \\ &\quad \times p(\text{selecting the } w\text{th value to split on}) \\ &= p(\text{GROW}) \frac{1}{B} \frac{1}{n_{\text{adj}}(b)} \times \frac{1}{n_{\text{cutpoint}}(b)}, \end{aligned}$$

and

$$\begin{aligned} q(U|U^*) &= p(\text{PRUNE}) \times p(\text{selecting node } \eta \text{ to prune from}) \\ &= p(\text{PRUNE}) \frac{1}{n_{\text{internal}^*}}, \end{aligned}$$

where $p(\text{GROW}) = 0.25$ and $p(\text{PRUNE}) = 0.25$ are the probability of BIRTH and DEATH move to be selected, and n_{internal^*} is the total number of internal nodes that has two terminal child nodes. Thus, we can derive the transition ratio to be

$$\frac{q(U|U^*)}{p(U^*|U)} = \frac{p(\text{PRUNE}) B n_{\text{adj}}(b) n_{\text{cutpoint}}(b)}{q(\text{GROW}) n_{\text{internal}^*}}.$$

Then, we follow Rosen et al. (2012) to draw the proposed terminal parameters β^* , τ^{2*} and latent variable a^* . For $\tau^2(a)$, let $\tau_b^2(a_b)$ denote the current $\tau^2(a)$ for the b th terminal node and a uniform distribution is used to generate new parameters $\tau_{b_l}^{2*}(a_{b_l}^*)$ and $\tau_{b_r}^{2*}(a_{b_r}^*)$ for the

left and right child. Specifically,

$$\begin{aligned}\tau_{b_l}^{2*} &= \tau_b^2 \times \frac{u_\tau}{1 - u_\tau}, & \tau_{b_r}^{2*} &= \tau_b^2 \times \frac{1 - u_\tau}{u_\tau} \\ a_{b_l}^* &= a_b \times \frac{u_a}{1 - u_a}, & a_{b_r}^* &= a_b \times \frac{1 - u_a}{u_a}\end{aligned}$$

where $u_\tau, u_a \sim U[0, 1]$. For β , an approximated normal distribution is proposed to generate the new parameters $\beta_{b_l}^*$ and $\beta_{b_r}^*$. Specifically, $(\beta_{b^*}^* | \tau_{b^*}^{2*}, U^*, U, \Phi) \sim N(\beta_b^{\max}, \Sigma_b^{\max})$, where

$$\beta_b^{\max} = \operatorname{argmax}_{\beta_{b^*}^*} p(\beta_{b^*}^* | \mathbf{R}_b, \tau_{b^*}^{2*}, U^*), \quad (11)$$

and

$$\Sigma_b^{\max} = \left\{ -(\partial^2 \log p(\beta_{b^*}^* | \mathbf{R}_b, \tau_{b^*}^{2*}, U^*)) / (\partial \beta_{b^*}^* \partial \beta_{b^*}^{\prime}) |_{\beta_{b^*}^* = \beta_b^{\max}} \right\}^{-1}, \quad (12)$$

where $p(\beta_{b^*}^* | \mathbf{R}_b, \tau_{b^*}^{2*}, U^*)$ is presented in Section 3.2, and b^* represents the left or right child of node b . We then have the proposed probability ratio

$$\begin{aligned}\frac{q(\beta, \tau^2 | U^*, \Phi^*, U)}{q(\beta^*, \tau^{2*} | U, \Phi, U^*)} &= \frac{q(\beta | \tau^2, U^*, \Phi^*, U) q(\tau^2 | U^*, \Phi^*, U) q(a | U^*, \Phi^*, U)}{q(\beta^* | \tau^{2*}, U, \Phi, U^*) q(\tau^{2*} | U^*, \Phi^*, U) q(a^* | U^*, \Phi^*, U)} \\ &= \frac{q(\beta_b)}{q(\beta_{b_l}^*) q(\beta_{b_r}^*) p(u)} \times \left| \frac{\partial(\tau_{b_l}^{2*}, \tau_{b_r}^{2*})}{\partial(\tau_b^2, u_\tau)} \right| \times \left| \frac{\partial(a_{b_l}^*, a_{b_r}^*)}{\partial(a_b, u_a)} \right|,\end{aligned}$$

where $p(u_\tau), p(u_a) = 1$, $q(\beta_b)$, $q(\beta_{b_l}^*)$ and $q(\beta_{b_r}^*)$ are the densities of the approximately normal distribution $N(\beta_b^{\max}, \Sigma_b^{\max})$ with the corresponding current and proposed τ^2 values.

The Jacobian of τ^2 and a are

$$\left| \frac{\partial(\tau_{b_l}^{2*}, \tau_{b_r}^{2*})}{\partial(\tau_b^2, u_\tau)} \right| = \frac{2\tau_b^2}{u_\tau(1 - u_\tau)}, \quad \left| \frac{\partial(a_{b_l}^*, a_{b_r}^*)}{\partial(a_b, u_a)} \right| = \frac{2a_b}{u_a(1 - u_a)}.$$

DEATH

The DEATH move is the inverse of the BIRTH move. Suppose b is the selected internal to be pruned by deleting the two child nodes b_l and b_r , the likelihood ratio for the proposed tree and the current tree is hence expressed as

$$\frac{p(\mathbf{R} | U^*, \Phi^*)}{p(\mathbf{R} | U, \Phi)} = \frac{p(\mathbf{R}_{b_1}, \dots, \mathbf{R}_{b_{n_b}}) | f_{jb}}{p(\mathbf{R}_{b_l, 1}, \dots, \mathbf{R}_{b_l, n_l} | f_{j b_l}) p(\mathbf{R}_{b_r, 1}, \dots, \mathbf{R}_{b_r, n_r} | f_{j b_r})},$$

which is the change from the two child nodes to the internal b node. The ratio of tree structure is presented as

$$\frac{p(U^*)}{p(U)} = \frac{1 - p_{\text{split}}(b)}{(1 - p_{\text{split}}(b_l))(1 - p_{\text{split}}(b_r))p_{\text{split}}(b)p_{\text{rule}}(b)},$$

and the ratio of transition

$$\frac{p(U|U^*)}{p(U^*|U)} = \frac{q(\text{GROW})n_{\text{internal}^*}}{q(\text{PRUNE})(B - 1)n_{\text{adj}}(b)n_{\text{cutpoint}}(b)},$$

where $B - 1$ is the number of terminal nodes for the proposed prune tree. For the proposed probability ratio, we draw terminal node parameters τ_b^{2*} and a_b^* by taking the inverse of the corresponding BIRTH move

$$\tau_b^{2*} = \sqrt{\tau_{b_l}^2 \tau_{b_r}^2}, \quad a_b^* = \sqrt{a_{b_l} a_{b_r}}.$$

The vector β_b^* is drawn from the approximately normal distribution $N(\beta_b^{\max}, \Sigma_b^{\max})$ given the proposed τ^{2*} value. Hence, the proposed probability ratio is

$$\frac{q(\beta, \tau^2 | U^*, \Phi^*, U)}{q(\beta^*, \tau^{2*} | U, \Phi, U^*)} = \frac{q(\beta_{b_l})q(\beta_{b_r})p(u)}{q(\beta_b^*)} \times \left| \frac{\partial(\tau_b^{2*}, u_\tau)}{\partial(\tau_{b_l}^2, \tau_{b_r}^2)} \right| \times \left| \frac{\partial(a_b^*, u_a)}{\partial(a_{b_l}, a_{b_r})} \right|,$$

where the Jacobian of τ^2 and a are

$$\left| \frac{\partial(\tau_b^{2*}, u_\tau)}{\partial(\tau_{b_l}^2, \tau_{b_r}^2)} \right| = \frac{u_\tau(1 - u_\tau)}{2\tau_b^{2*}} = 2(\tau_{b_l} + \tau_{b_r})^2,$$

$$\left| \frac{\partial(a_b^*, u_a)}{\partial(a_{b_l}, a_{b_r})} \right| = \frac{u_a(1 - u_a)}{2a_b^*} = 2(\sqrt{a_{b_l}} + \sqrt{a_{b_r}})^2.$$

CHANGE

A CHANGE move is to change two terminal nodes to a pair of new child nodes by changing the split rule of their parent node. The observations within each terminal node of the proposed tree can be different from the current tree. Thus, the likelihood ratio is

$$\frac{p(\mathbf{R}|U^*, \Phi^*)}{p(\mathbf{R}|U, \Phi)} = \frac{p(\mathbf{R}_{l,1}, \dots, \mathbf{R}_{l,n^{l^*}} | f_{j_{b_l^*}})p(\mathbf{R}_{r,1}, \dots, \mathbf{R}_{r,n^{r^*}} | f_{j_{b_r^*}})}{p(\mathbf{R}_{l,1}, \dots, \mathbf{R}_{l,n^l} | f_{j_{b_l}})p(\mathbf{R}_{r,1}, \dots, \mathbf{R}_{r,n^r} | f_{j_{b_r}})},$$

where n^{l^*} and n^{r^*} are the number of observations in the new left and the new right child nodes. The tree structure ratio for the CHANGE move is

$$\frac{p(U^*)}{p(U)} = \frac{(1 - p_{\text{split}}(b_{l^*}))(1 - p_{\text{split}}(b_{r^*}))p_{\text{split}}(b^*)p_{\text{rule}}(b^*)}{(1 - p_{\text{split}}(b_l))(1 - p_{\text{split}}(b_r))p_{\text{split}}(b)p_{\text{rule}}(b)},$$

since the depth of the children nodes does not change, the split probability for each node stays the same. The only change is the number of the available cutpoints of the new variable, which can be different from the current variable. Therefore, the tree structure ratio is

$$\frac{p(U^*)}{p(U)} = \frac{n_{\text{cutpoint}}(b)}{n_{\text{cutpoint}}(b^*)},$$

where $n_{\text{cutpoint}}(b^*)$ is the number of available cutpoints for the proposed variable. The transition probability from current tree to the proposed tree is

$$\begin{aligned} p(U^*|U) &= p(\text{CHANGE}) \times p(\text{selecting node } b \text{ to change}) \\ &\quad \times p(\text{selecting the new predictor to split on}) \\ &\quad \times p(\text{selecting the new cutpoint to split on}). \end{aligned}$$

The calculation of the $p(U|U^*)$ is similar with $p(U^*|U)$ except that the number of available cutpoints can be different. So the transition ratio is

$$\frac{p(U|U^*)}{p(U^*|U)} = \frac{n_{\text{cutpoint}}(b^*)}{n_{\text{cutpoint}}(b)}.$$

From the results above, the transition ratio and the tree structure ratio are cancelled in the representation of Equation (10). So the acceptance ratio for the CHANGE step is only related to the likelihood, prior probability and the proposed probability of terminal node parameters. Two-step Gibbs sampling is used to draw new terminal node parameters. The $\beta_{b^*}^*$ is drawn from the normal approximation $N(\beta_b^{\max}, \Sigma_b^{\max})$ given the current $\tau_{b^*}^2$, and a_{b^*} and $\tau_{b^*}^2$ are draw from their full conditional distributions. The MCMC algorithm draws a_{b^*} first and then updates $\tau_{b^*}^2$.

Web Appendix B: Additional Results

Additional simulation results and the gait maturation analysis are shown in the following section. We set $M = 5$, $L = 100$, and $T = 250$ when modeling the simulated data by using 10,000 iterations with the first 5,000 iterations discarded as burn-in. Also, we display the distribution of mean run times for the three simulations and the number of bottom nodes for

different number of time series (L) and length of time series (T) of AR-Friedman simulation to illustrate the effect of L and T on the computation time.

Estimation and Convergence Diagnostics of Simulations

To show the estimation accuracy of the proposed method, for the AR-Friedman simulation setting, where the covariates influence the power spectrum in more complicated ways, We randomly selected eight observations for illustration, and Figure 5 shows the estimated log power spectrum of the selected observations. For the Adjusted-AdaptSPEC-X simulation, two observations are randomly selected within each of the four regions shown in Figure 6. The corresponding estimation results for the eight observations are shown in Figure 7. We observe that the proposed model performs very well in capturing the true trend of the power spectrum in both simulation settings. The convergence diagnostic plots for all three settings are shown in Figure 8, Figure 9, and 10 separately, which appear to converge after 5000 burn-in iterations.

[Figure 5 about here.]

[Figure 6 about here.]

[Figure 7 about here.]

[Figure 8 about here.]

[Figure 9 about here.]

[Figure 10 about here.]

Convergence Diagnostics of Gait Maturation

Convergence diagnostics for the gait maturation data analysis are shown in Figure 11. While the sampler appears to converge more slowly than the simulation settings, the sampler appears to converge after 5,000 burn-in iterations.

[Figure 11 about here.]

Posterior Probability of Inclusion for Sparse Covariate Effects

To demonstrate variable selection using the Dirichlet prior, effects on high-dimensional data as described in Section 5.4, posterior probabilities of model inclusion under the uniform and Dirichlet priors for important variables and noise variables from a single run with $L = 500$, $T = 250$, and $M = 50$ is presented in Figure 12.

[Figure 12 about here.]

Tree Size and Run Time

The distribution of mean run times for the three simulations is shown in Figure 13. We observe that the tree size tends to increase as both the number of time series (L) and the length of time series (T) increase. Figure 14 shows the total number of bottom nodes for four different settings for AR-Friedman simulation. The total number of bottom nodes for $L = 500, T = 500$ is over 50 while it is about 13 for $L = 100, T = 100$. This can help explain why the mean run times grow more slowly in L compared to T , as the mean number of time series belonging to each terminal node increases modestly.

[Figure 13 about here.]

[Figure 14 about here.]

Web Appendix C: R Implementation of the Proposed Adaptive Bayesian Sum of Trees Model

BayesSumOfTreesSPEC.zip contains a README file with instructions for running a demo of the Bayesian sum of trees model on the three simulation settings and a description of the files provided. For the simulation settings, this folder includes the R code needed to generate the simulated data, produce convergence diagnostics, and visualize the estimated

covariate-dependent conditional power spectrum. For the application, this folder includes the original publicly-available data (Goldberger et al., 2000), R code for data pre-processing following Hausdorff et al. (1999), processed data used for analysis, and R code for producing the convergence diagnostics and ALE plots. Computationally-intensive aspects of the code, such as the optimization required to approximate the posterior distribution of the spline coefficients and building and modifying the tree structures within the MCMC sampler, are written in C++ using RcppArmadillo (Eddelbuettel and Sanderson, 2014) for more efficient computation and reduced run times.

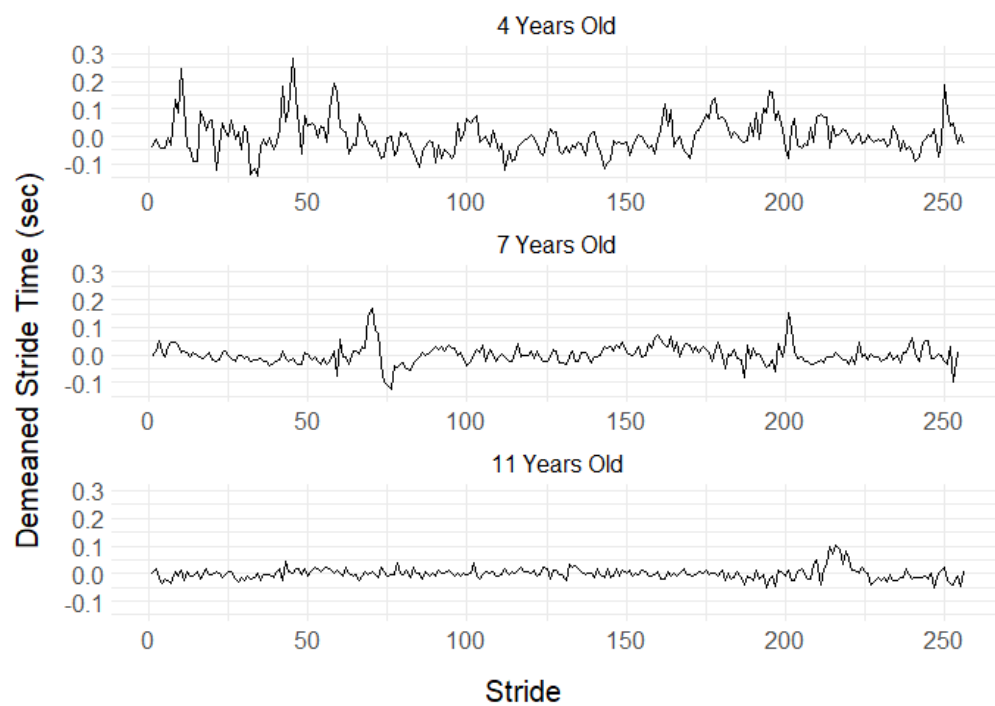


Figure 1. Demeaned stride interval time series for three participants in the gait maturation study ages 4, 7, and 11 years old.

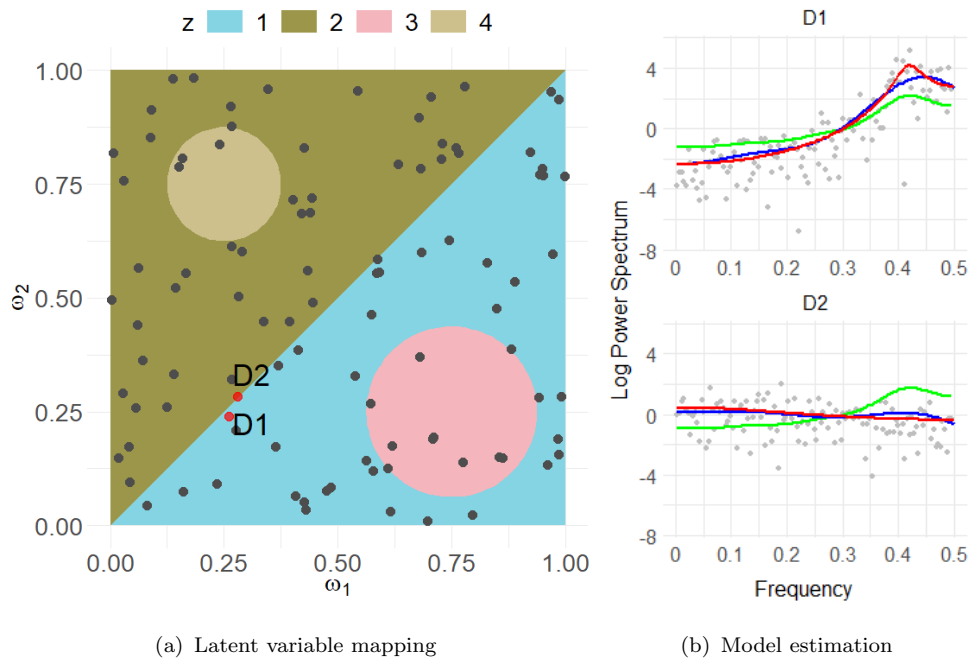


Figure 2. (a) presents the mapping of covariate values ω_1 and ω_2 to latent variable values z for the Adjusted-AdaptSPEC-X simulation setting. D1 and D2 denote two simulated time series with similar covariate values that are mapped to different latent variable values corresponding to different power spectra. For these two realizations, (b) displays the true log power spectra (red lines), log periodogram ordinates (gray points), and estimated log power spectra using the proposed Bayesian sum of trees model (blue lines) and the AdaptSPEC-X model (green lines).

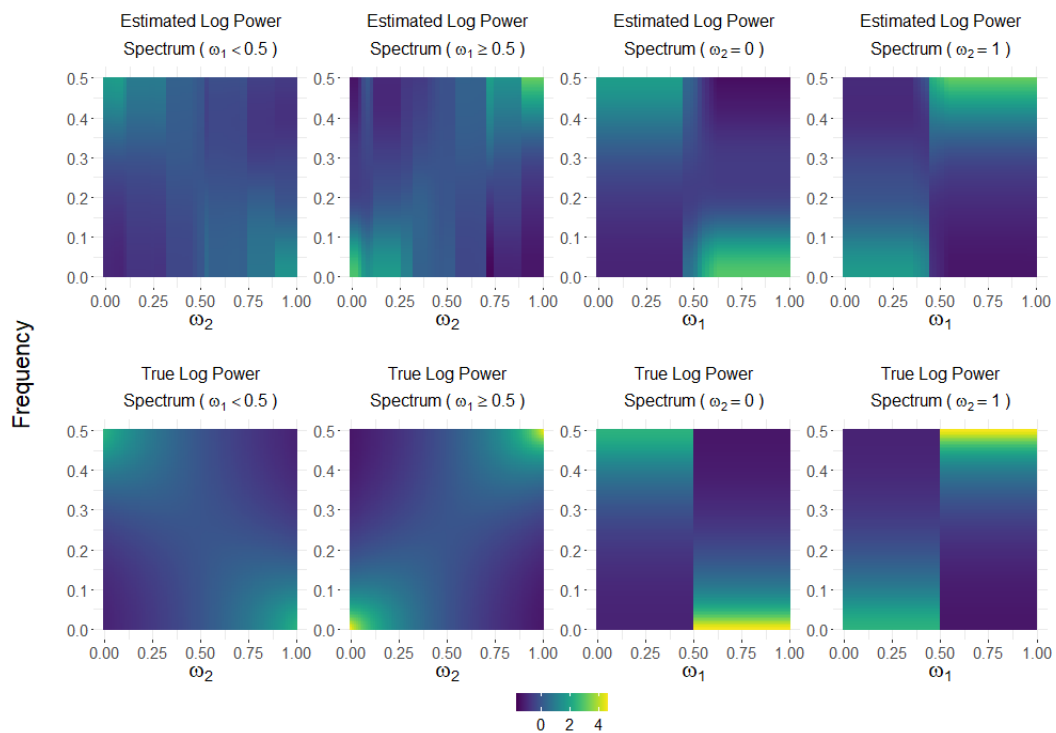


Figure 3. Estimated and true covariate-dependent conditional log power spectrum for one run of the Abrupt+Smooth simulation setting. The first two columns contain the estimated and true covariate-dependent power spectrum conditional on $\omega_1 < 0.5$ and $\omega_1 \geq 0.5$ respectively; The last two columns display the estimated and true covariate-dependent power spectrum conditional on $\omega_2 = 0$ and $\omega_2 = 1$ respectively.

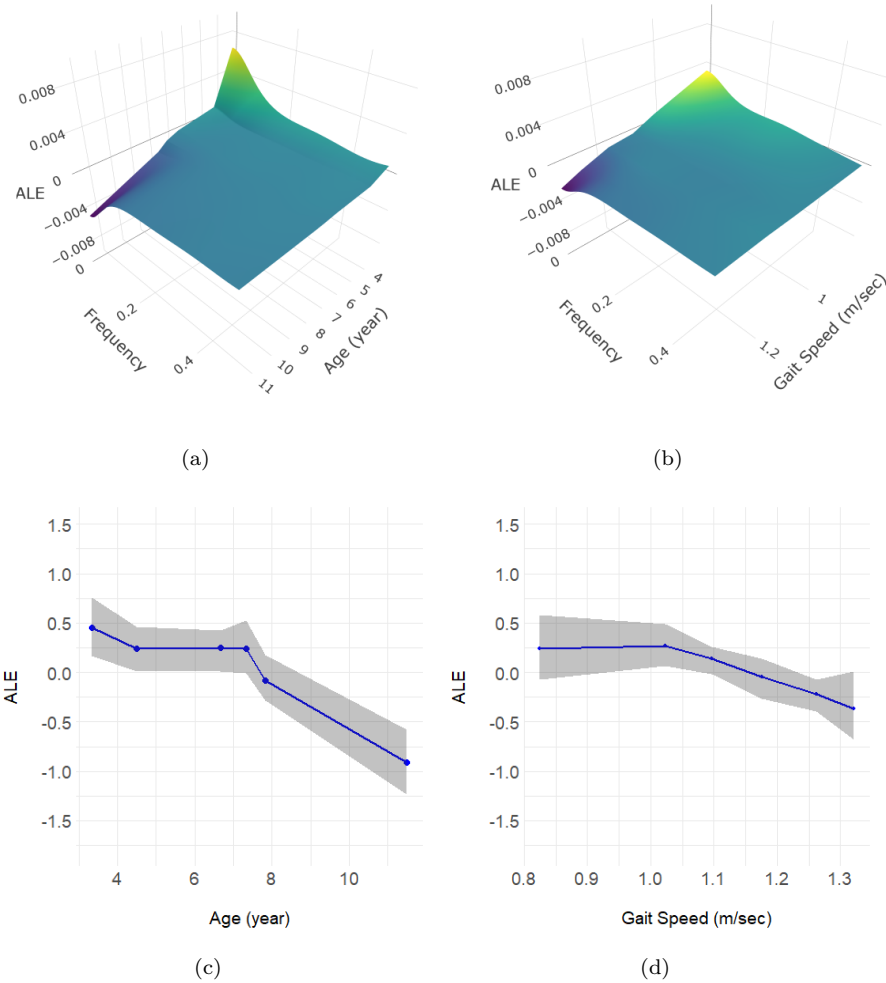


Figure 4. Posterior mean of ALE for age (a) and gait speed (b) effects on the power spectrum and posterior mean of ALE for age (c) and gait speed (d) on LF/HF ratio (blue dotted line) with 95% pointwise credible intervals (shaded gray region).

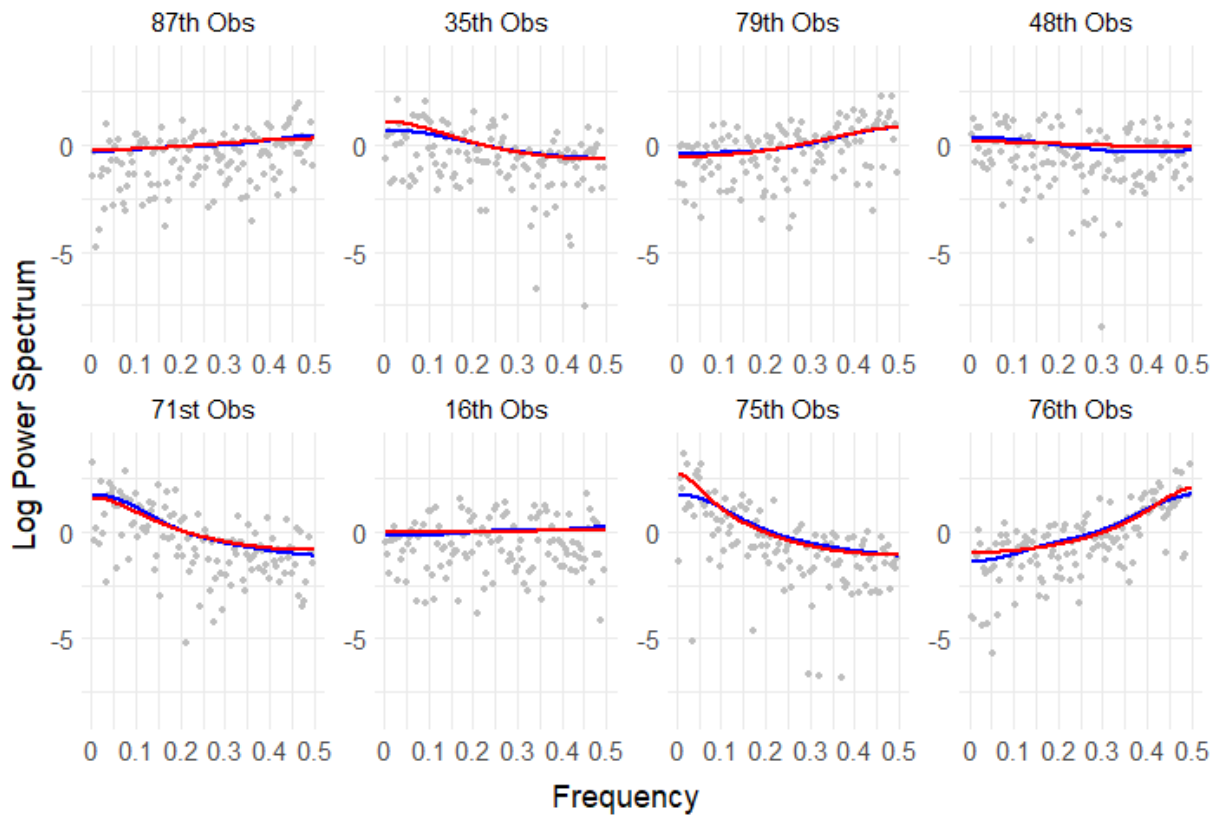


Figure 5. The estimated (blue line) and the true (red line) log power spectrum of the eight randomly selected time series for the AR-Friedman simulation. The corresponding log periodogram ordinates are shown with gray dots.

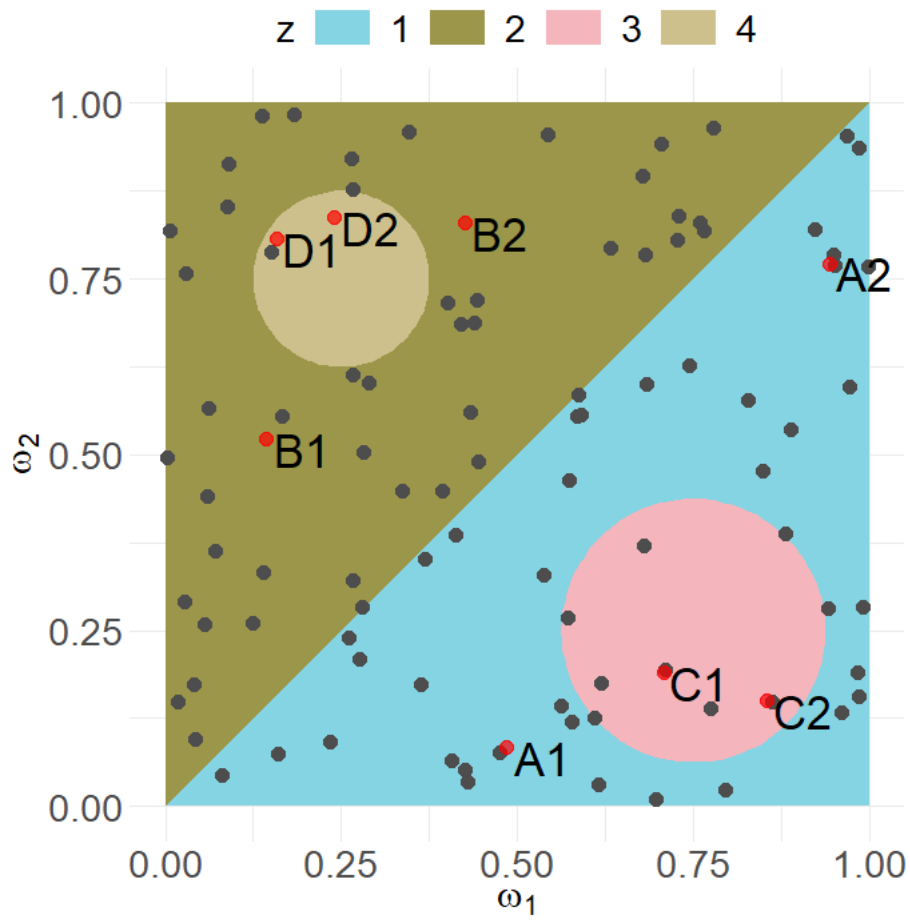


Figure 6. The mapping of the covariates ω_1 and ω_2 to the latent variable z for the Adjusted-AdaptSPEC-X simulation setting with eight specific time series (red dots).

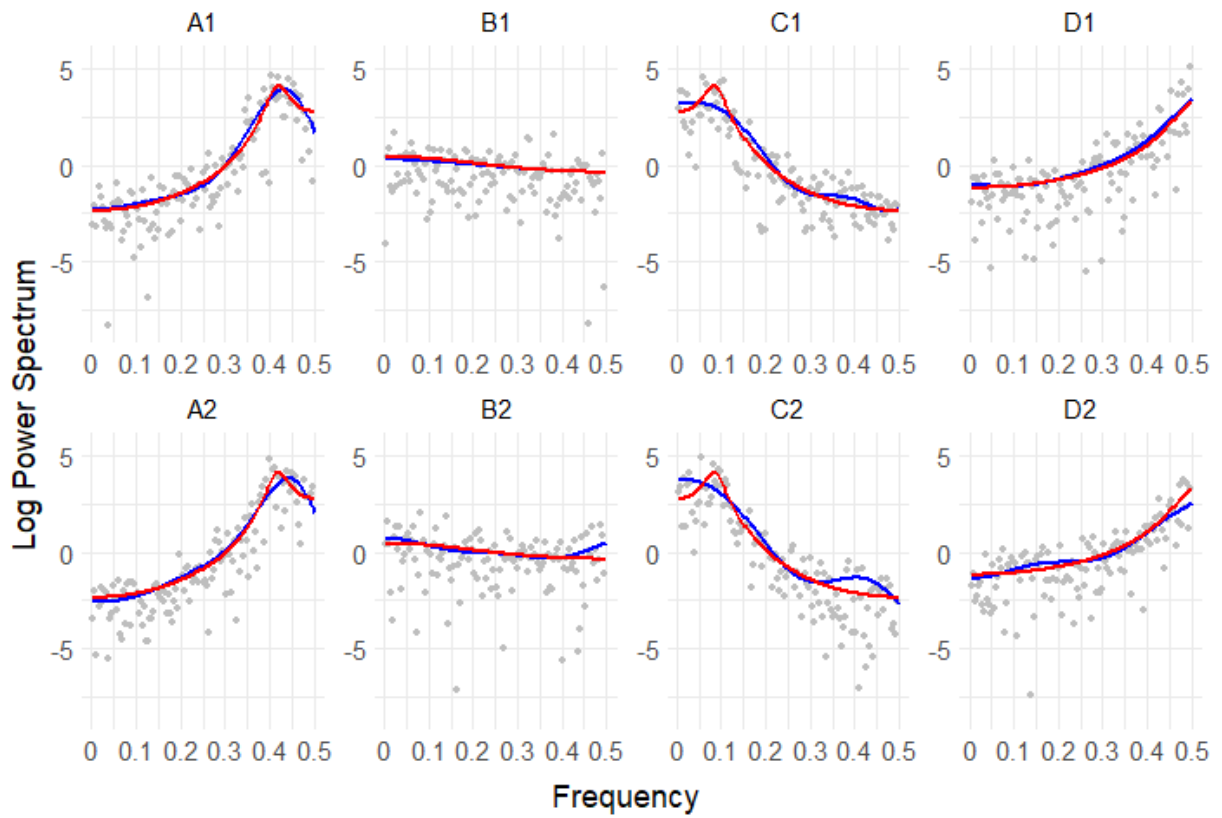


Figure 7. The estimated (blue line) and the true (red line) log power spectrum of the eight time series denoted in Figure 6. The corresponding log periodogram ordinates are shown with gray dots.

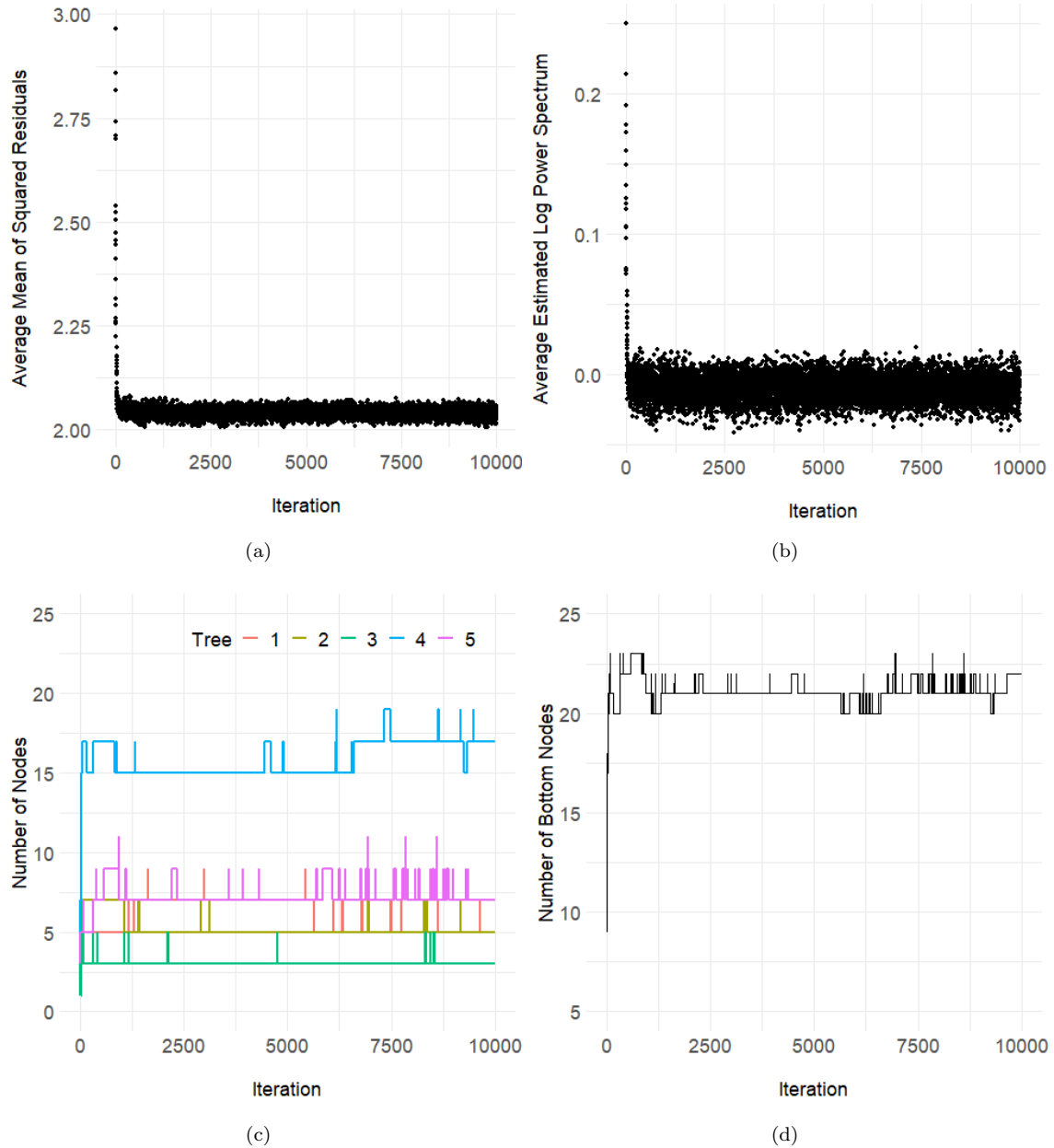


Figure 8. Convergence diagnostic plots for the Abrupt+Smooth simulation for one replication: (a) average mean squared residuals across frequencies and all time series; (b) average estimated log power spectrum across frequencies and all time series; (c) total number of nodes for each of the five trees; (d) total number of bottom nodes across all five trees.

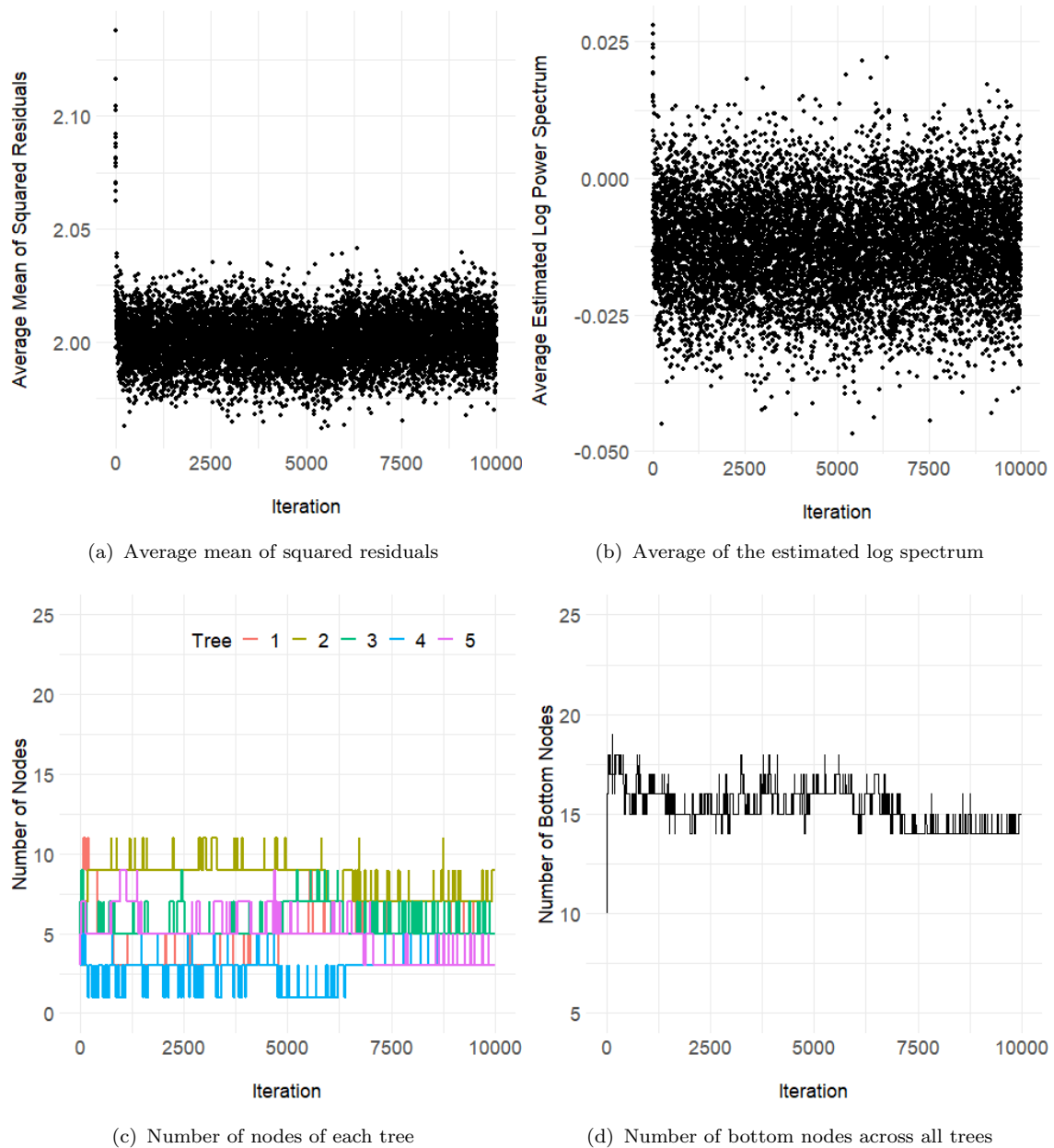


Figure 9. Convergence diagnostics for the AR-Friedman simulation for one replication. Plot (a) contains trace plots of the average mean squared residuals across all time series; Plot (b) shows the average estimated log power spectrum across frequencies and all time series for each iteration; Plot (c) is the trace plots of the total number of nodes for each of the five trees separately (c); Plot (d) is the total number of bottom nodes across all five trees.

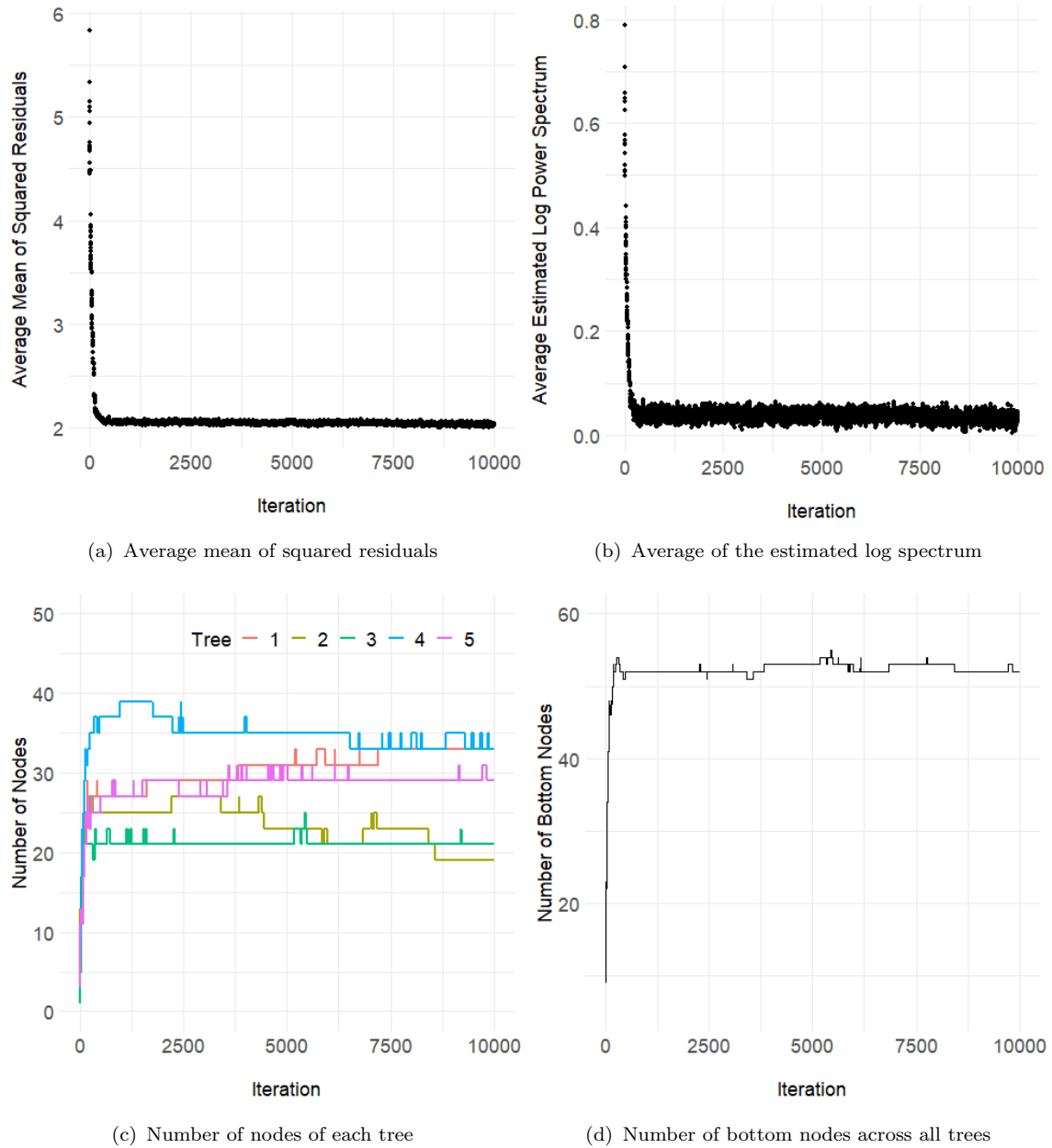


Figure 10. Convergence diagnostics for the Adjusted-AdaptSPEC-X simulation for one replication. Plot (a) contains trace plots of the average mean squared residuals across all time series; Plot (b) shows the average estimated log power spectrum across frequencies and all time series for each iteration; Plot (c) is the trace plots of the total number of nodes for each of the five trees separately (c); Plot (d) is the total number of bottom nodes across all five trees.

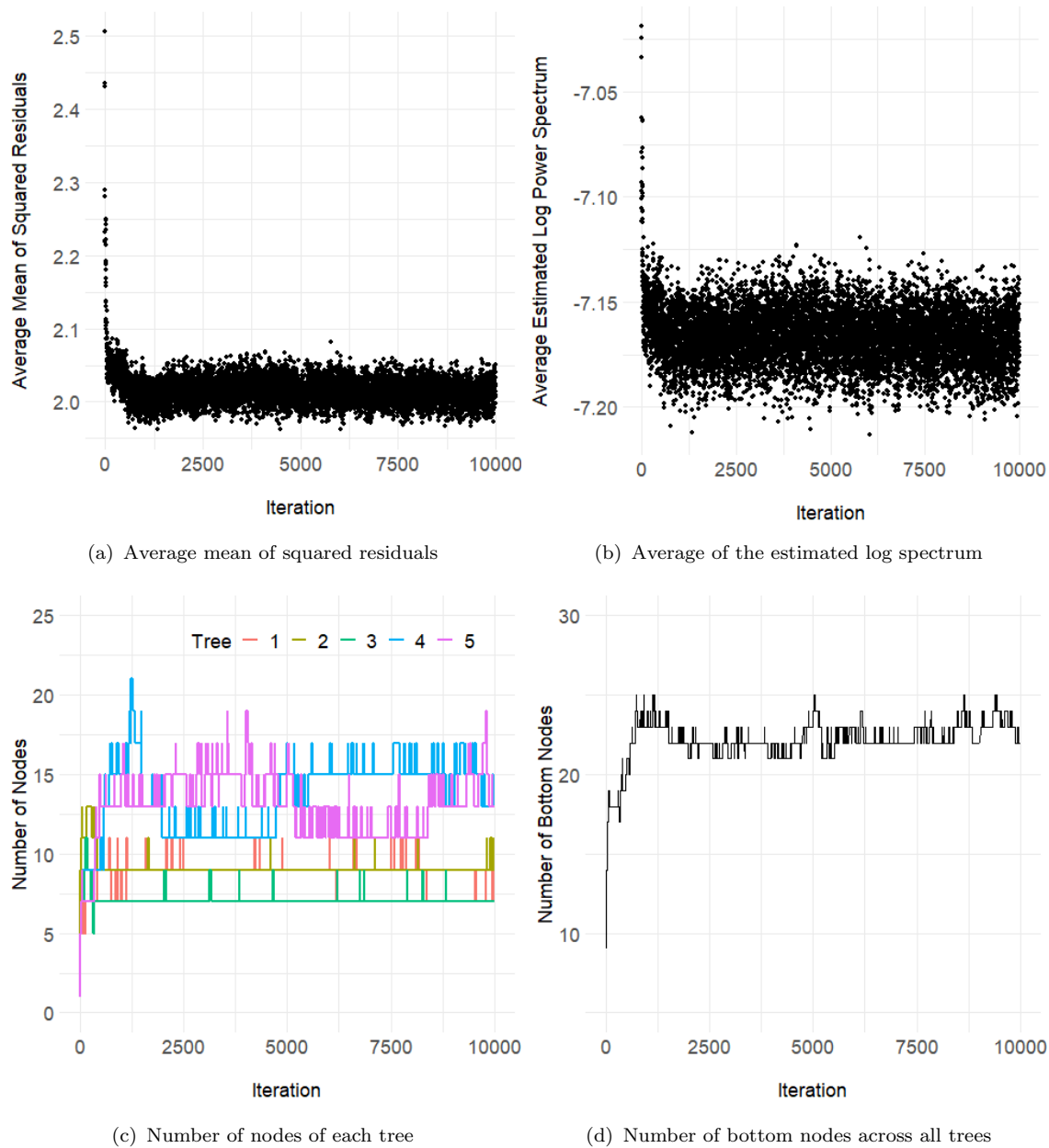


Figure 11. Convergence diagnostics for the gait maturation data analysis. Plot (a) contains trace plots of the average mean squared residuals across all time series; Plot (b) shows the average estimated log power spectrum across frequencies and all time series for each iteration; Plot (c) is the trace plots of the total number of nodes for each of the five trees separately (c); Plot (d) is the total number of bottom nodes across all five trees.

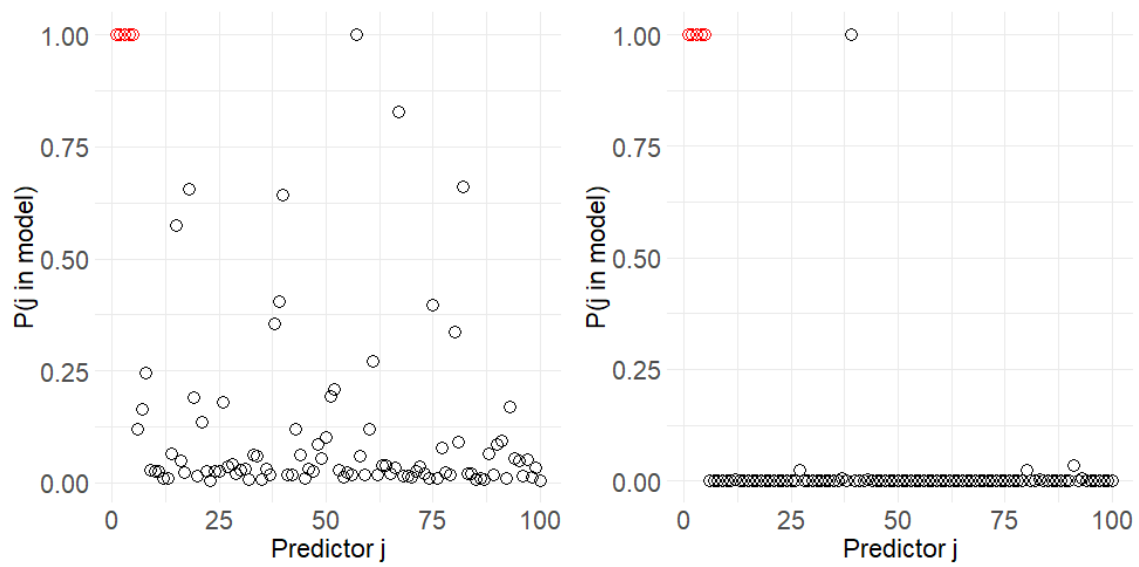


Figure 12. Posterior probabilities of model inclusion under the uniform (left) and Dirichlet (right) priors for important variables (red) and noise variables (black).

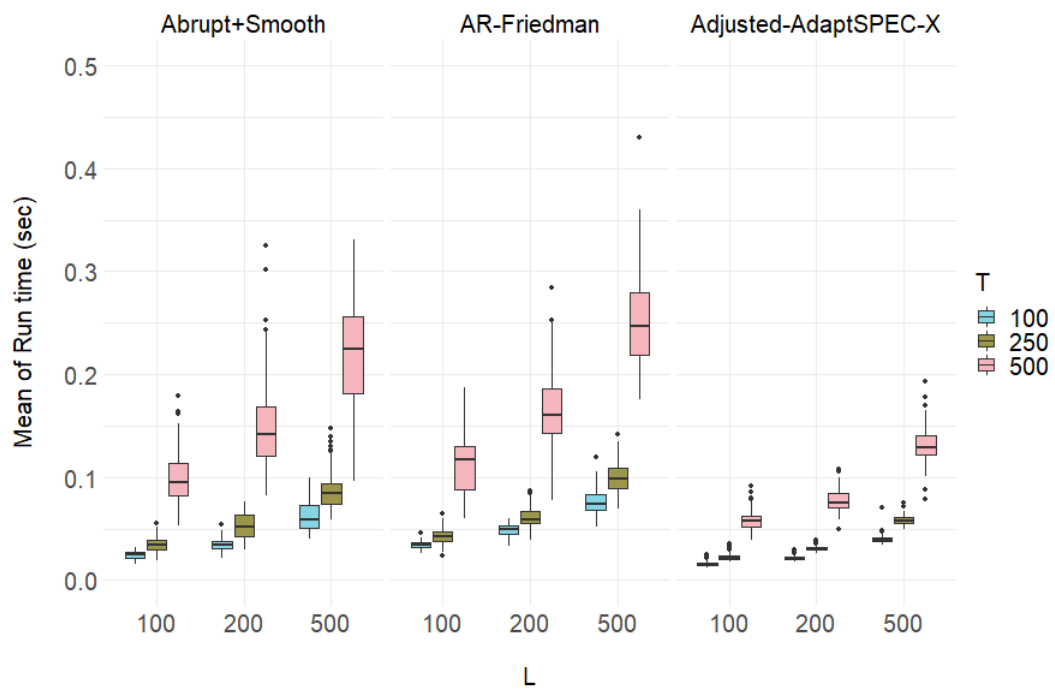


Figure 13. The distribution of mean run times in seconds for a single tree update over 100 replicates of the three simulations with $M = 5$ trees.



Figure 14. The total number of bottom nodes over iterations for four runs with different L and T for the AR-Friedman simulation setting.

Table 1

Mean and standard deviation of MSE over 100 replications for three simulation settings with different lengths (T) and number (L) of time series. Results are presented for the proposed Bayesian sum of trees model (top) with number of trees $M = 5$ and the AdaptSPEC-X model (bottom) with mixture components $C = 50$.

		Abrupt+Smooth	AR-Friedman	Adj. AdaptSPEC-X
L	T	Proposed Bayesian Sum of Trees Model		
100	100	0.0406(0.0062)	0.0386(0.0059)	0.1475(0.0249)
100	250	0.0217(0.0031)	0.0226(0.0030)	0.0762(0.0102)
100	500	0.0138(0.0019)	0.0153(0.0019)	0.0528(0.0063)
200	100	0.0320(0.0052)	0.0338(0.0042)	0.1446(0.0202)
200	250	0.0173(0.0030)	0.0197(0.0020)	0.0719(0.0070)
200	500	0.0118(0.0023)	0.0138(0.0015)	0.0483(0.0050)
500	100	0.0238(0.0030)	0.0276(0.0022)	0.1348(0.0140)
500	250	0.0124(0.0015)	0.0160(0.0013)	0.0663(0.0077)
500	500	0.0085(0.0013)	0.0119(0.0012)	0.0452(0.0060)
L	T	AdaptSPEC-X Model		
100	100	0.0576(0.0113)	0.0529(0.0082)	0.6334(0.1256)
100	250	0.0437(0.0108)	0.0406(0.0073)	0.5595(0.1163)
100	500	0.0412(0.0126)	0.0377(0.0070)	0.5394(0.1174)
200	100	0.0510(0.0087)	0.0474(0.0058)	0.5182(0.0735)
200	250	0.0398(0.0089)	0.0372(0.0060)	0.4453(0.0657)
200	500	0.0378(0.0093)	0.0365(0.0061)	0.4240(0.0619)
500	100	0.0466(0.0053)	0.0398(0.0039)	0.4631(0.0445)
500	250	0.0379(0.0051)	0.0323(0.0049)	0.4012(0.0410)
500	500	0.0370(0.0050)	0.0319(0.0047)	0.3851(0.0369)